Received: 10 January 2022 | Revised: 15 June 2022 | Accepted: 27 June 2022

DOI: 10.1111/bre.12697

Basin Research | IAS EAGE | WILEY

RESEARCH ARTICLE

Seismic characterization and depositional significance of the Nahr Menashe deposits: Implications for the terminal phases of the Messinian salinity crisis in the north-east Levant Basin, offshore Lebanon

S. M. Mainul Kabir[1] | **David Iacopini**[2] | **Adrian Hartley**[1] | **Vittorio Maselli**[3] | **Davide Oppo**[4]

[1]School of Geosciences, University of Aberdeen, Aberdeen, UK

[2]Department of Earth, Environmental and Resources Science, University of Naples Federico II, Naples, Italy

[3]Department of Earth and Environmental Sciences, Dalhousie University, Halifax, Nova Scotia, Canada

[4]Sedimentary Basins Research Group, School of Geosciences, University of Louisiana at Lafayette, Lafayette, Louisiana, USA

Correspondence
S. M. Mainul Kabir, School of Geosciences, University of Aberdeen, Aberdeen, UK.
Email: r01smmk@abdn.ac.uk

Abstract

Over the last decade, there has been a resurgence of interest in the climatic and tectonic mechanisms that drove the Messinian salinity crisis (MSC) and the associated deposition of thick evaporites. The MSC represents an unprecedented palaeoceanographic change that led to a very short (ca. 640 kyr) ecological and environmental crisis. However, across the Levantine offshore basin, the sedimentological nature of the top evaporitic units and the mechanisms that controlled the transition from a hypersaline evaporitic unit to brackish deposits (final MSC stage 3) are still disputed. Here, we re-evaluate the deposits associated with the terminal phase of the MSC, named in offshore Lebanon as the Nahr Menashe Unit (NMU). We describe the NMU seismic facies, characterize and map its internal seismic stratigraphy and provide a new interpretation of its depositional environment, which persisted during the late Messinian and then evolved through a regional reflooding event. The base of the NMU overlies semicircular depressions, randomly distributed linear marks and surface collapse features, which are indicative of a period of intense evaporite dissolution. The NMU seismic facies observed from the slope to the deep part of the basin support the interpretation of a layered salt-evaporite-sand depositional system subject to complex reworking, dissolution, deposition and final erosion. A drainage network of valleys and complex tributary channels incising into the top NMU shows marked erosional characteristics, which indicate a dominant southwards sediment transfer following deposition of the NMU. The drainage network was subsequently infilled by layered sediments interpreted here to represent the post-MSC marine sediments. Our analysis adds important details regarding previous interpretations of the NMU as fluvial in origin. Specifically, the presence of subcircular, linear dissolution features coupled with mound-like features indicates that the NMU is composed dominantly of evaporites that were subject to dissolution prior to erosion associated

with the drainage network. The NMU is interpreted to represent the deposition/re-deposition of a mixed evaporite-siliciclastic succession in a shallow marine or lacustrine environment during the tilting of the offshore Lebanese basin.

KEYWORDS
dissolution, incise, Levant, Messinian, passive infill, seismic facies

Highlights

- We describe and characterize seismic facies within the terminal deposits of the Messinian salinity crisis event.
- The NMU seismic facies suggest deposition of a mixed package of evaporites, carbonates and clastics in a marginal marine or lacustrine setting subject to complex reworking, dissolution and subsequent erosion.
- Our seismic data interpretation of the Nahr Menashe Unit (NMU) challenges previous interpretations as fluvial in origin.
- An erosional drainage network comprising trunk valleys supplied by tributary channel networks incise the top of the NMU.
- Seismic reflection patterns within the valley/channel network indicate a passive infill during a rapid marine transgressive event.

1 | INTRODUCTION

The isolation of the Mediterranean Sea from the Atlantic Ocean during the Messinian salinity crisis (MSC; Ryan, 1978) led to the rapid deposition of a halite-dominated evaporite sequence (Haq et al., 2020; Roveri et al., 2016; Ryan, 2011), which is up to 2 km thick in the deeper parts of the Eastern Mediterranean region (Haq et al., 2020; Ryan & Cita, 1978, Figure 1a). Despite a long research history (Haq et al., 2020; Hsü et al., 1973; Lofi et al., 2011; Netzeband et al., 2006; Roveri et al., 2014), the scientific community is still divided on how and why this enigmatic event ended (Andreeto et al., 2021; Haq et al., 2020; Meilijson et al., 2019; Popescu et al., 2021; Roveri et al., 2014). This uncertainty is partly due to significant variations in the magnitude and duration phase of the evaporite deposition across the basins (Camerlenghi et al., 2019). As a consequence, the Messinian deposits record different tectonostratigraphic histories in different sub-basins of the Mediterranean (see Amadori et al., 2018; Andreeto et al., 2021; Roveri et al., 2014). From a seismic stratigraphic perspective, three distinct seismic units have been identified in the Western Mediterranean Basins (Lofi et al., 2011), whereas in the Eastern Mediterranean region, one single Mobile Unit (MU) (Camerlenghi et al., 2019; Lofi et al., 2011; Netzeband et al., 2006; Roveri et al., 2014) has been recognized, containing the alternation of high-amplitude coherent reflectors and seismically transparent layers (Figure 2a). In the Levant area, where the MU reaches its maximum thickness, six subunits have been recognized by Cartwright et al. (2012) and further described using a velocity model for the transparent and reflective layers (Feng et al., 2016; Gvirtzman et al., 2013). In offshore Israel, Feng et al. (2016) presented a well log interpretation model showing that the transparent units have distinctly higher velocities (4200–4400 m/s) than the reflective parts (3800–4000 m/s). They interpreted the higher velocity packages as thick halite layers with intra-salt reflective horizons, with lower velocities considered to represent a mixture of salt and clastic deposits. Other workers (Cartwright & Jackson, 2008; Gradmann et al., 2005) suggested that the intra-salt reflective layers are composed of anhydrite or gypsum. Gvirtzman et al. (2017) used gamma ray and resistivity logs together with seismic data to define a new package (named Unit 7) which forms the uppermost unit of the Messinian evaporites bounded between two key horizons, the Intra-Messinian truncation surface (IMTS) (Gvirtzman et al., 2017) and the Messinian Zanclean boundary (Figure 2). No cuttings are present in the deep basin for Unit 7 but landward there is data from the Judean Hills, Onshore Israel (Gardosh et al., 2008). Here, the unit equivalent to this uppermost seismic package appears to be represented by the anhydrite-siliciclastic Mavqiim Formation, overlain by the evaporite-free, Lago-Mare, Afiq Formation (Gardosh et al., 2008; Gvirtzman et al., 2017). Offshore Israel, this unit is interpreted to comprise alternating anhydrite, sand and clay layers (Ben Moshe et al., 2020). In the Lebanese Levant Basin, information regarding the lithological nature of the termination of the MSC is limited due to a lack of publicly available well data and core materials. Consequently, the stratigraphic framework and interpretation of the MSC event in the Lebanese section of the Levant basin are still exclusively dependent on geophysical methods (primarily

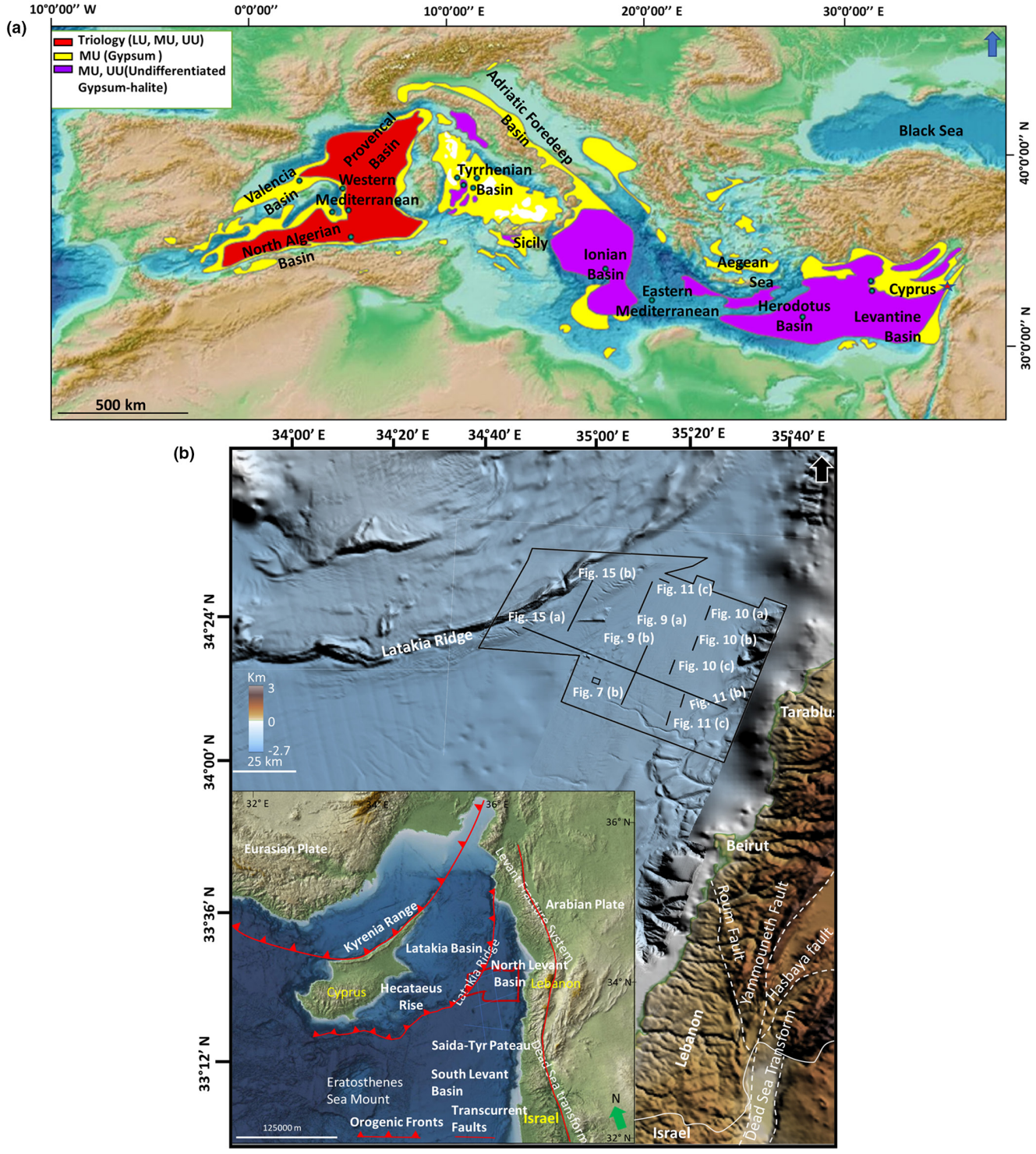

FIGURE 1 (a) Distribution of Messinian Evaporites in Mediterranean Basins and DSDP-ODP borehole locations (⬭) which recovered Messinian deposits (source Roveri et al., 2014) study area ★. (b) Location map of the study area showing topography, bathymetry and major structural elements. 2D seismic lines by a blue line and 3D seismic cube by the red box (used Petrel GIS service for map generation). The zoomed part indicates the 3D fence, and embedded lines are the position of different seismic sections used in this paper. Bathymetry is derived from the 3D seismic data, GEBCO and EDMOnet databases.

interpretation of seismic reflection data). Across the central north Levantine basin, the supra evaporitic deposits above the IMTS have been mapped and named by Madof et al. (2019) as the Nahr Menashe deposits. For reference, Madof et al. (2019) renamed the IMTS, sensu Gvirtzman et al. (2017), and previously termed the TS/TES by Lofi et al. (2011) as the 'Intermediate Erosion Surface'. Given its stratigraphic position, the Nahr Menashe has been

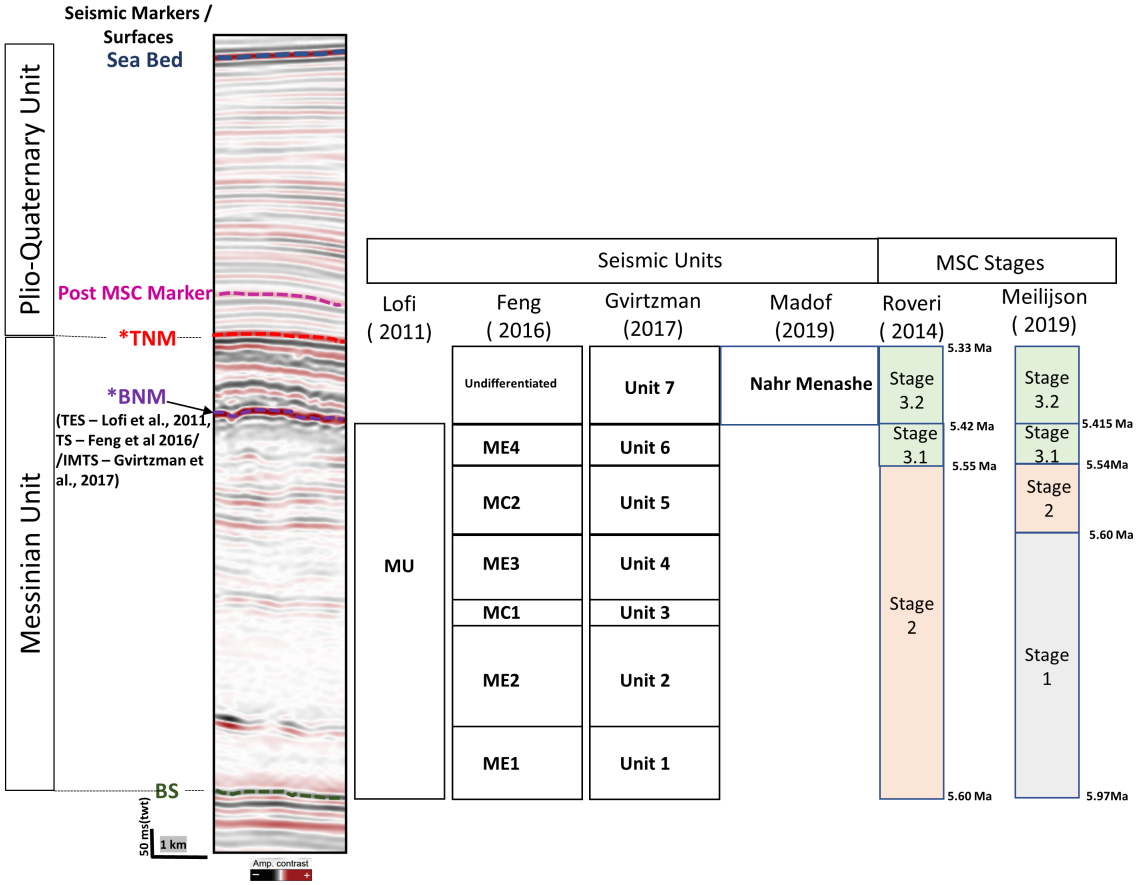

FIGURE 2 (a) Seismic stratigraphy and chronostratigraphy of the Levant Basin modified after Krickham et al. (2020), stratigraphic framework, nomenclatures and key markers are (from Feng et al., 2016; Gvirtzman et al., 2017; Lofi et al., 2011) correlated with chronostratigraphic models of Roveri et al. (2014) and Meilijson et al. (2019). *TNM, Top Nahr Menashe; BNM, Bottom Nahr Menashe. (b) Seismic markers of the study area with a positive filling wiggle, as all the hard kicks associate with red colour trough so data displayed reverse polarity.

interpreted to be Late Messinian in age, equivalent to the upper part of stage 3 (3.2) of Roveri et al. (2014), to Unit 7 proposed by Gvirtzman et al. (2017) in Israel or Unit 3.2 in the new stratigraphic scheme proposed by Meilijson et al. (2019) (Figure 2). Stratigraphically, this Unit is commonly considered equivalent to the second and third stages of the 'Lago-Mare' period (Andreetto et al., 2021). The interpretation (based on seismic and wireline data) proposed for these top Messinian deposits mapped across the central north levant and the Cyprus basin area varies from fluvial deposits subject to subaerial exposure that pass down-dip into lacustrine deposits (Madof et al., 2019), to shallow-marine deposits with subaqueous dissolution and a truncation surface at the base (Gvirtzman et al., 2017; Kirkham et al., 2017). In this paper, using a newly released 3D seismic data set, we reassess stage 3 of the MSC (sensu Roveri et al., 2014) in the north-eastern Levant Basin, with respect to the description and interpretation of the uppermost Messinian deposits (approximately equivalent to Unit 7 or Unit 3.2). For simplicity, the seismic package defining the Nahr Menashe deposits will here be named the Nahr Menashe Unit (NMU). Here, we describe, illustrate and discuss the distinctive seismic facies assemblages that characterize the internal stratigraphy of the NMU. We then extend our interpretation to explain the timing and nature of the distinctive erosive and dissolution features that are present at the base and across the intra-NMU layers to reconstruct the paleodepositional history of this seismic unit. Our results fine-tune the complexity of the NMU and shed new light on the terminal phases of the MSC during this widely debated period in the history of the Mediterranean Sea.

2 | GEOLOGICAL SETTING

The study area is located in the East Mediterranean Sea, Levant Basin and offshore Lebanon (Figure 1b). It is bordered by the Latakia Ridge to the northwest, the Levant Fracture System (Dead Sea Transform Zone) to the east, the Eratosthenes Seamount to the west, and the edge of the Nile delta deep-sea cone to the southwest (offshore Israel). The Levant Basin and surrounding area have undergone a long and complex tectonic history.

This includes Permian to Early Jurassic polyphase rifting (Gardosh et al., 2010; Garfunkel, 1998; Petrolink et al., 2001) linked to the opening of the Neotethys Ocean (Nader et al., 2011), a passive margin development in the Late Jurassic, followed by plate collision and associated subduction in the Late Cretaceous that created the Latakia Ridge as a part of the Cyprus Arc System (Robertson et al., 2012) with ophiolite emplacement and orogenesis in the Late Maastrichtian (Hawie et al., 2013; Hsü et al., 1973; Petrolink et al., 2001; Robertson, 1998). Across the Eastern Mediterranean and its marginal zones, the Late Cretaceous collision (which continues to the present day) led to a topographical inversion of early Mesozoic normal faults and sets of asymmetric folds along the basin margin (Syrian arc structures (Garfunkel, 1998; Hardy et al., 2010)). In the Late Miocene, as a response to the opening of the Gulf of Aden and Red Sea (Beydoun, 1999; Hawie et al., 2013) compression moved to the onshore Dead Sea Transform (Kartveit et al., 2019) along the Levant Fracture System and also reactivated the Latakia Ridge as a sinistral transpressional feature (Hall et al., 2005). After the Messinian, as a consequence of transpressive movement along the North–South Levant fracture system driven by the westward migration of the Anatolian plate (Hawie et al., 2013), the eastern margin of the Levant basin become progressively uplifted (Gvirtzman et al., 2013) from the Miocene to late Pleistocene (Ghalayini et al., 2018; Matmon et al., 1999).

A stratigraphic scheme for the northern Levant Basin based on good data has yet to be published, therefore correlation has been guided using information from the southern Levant Basin (Gvirtzman et al., 2013; Meilijson et al., 2019; Walley, 1997). Sedimentary sequences beneath the Messinian salt deposits are composed primarily of carbonate–siliciclastic sediments sourced from both the proto-Nile delta (Gardosh & Druckman, 2005; Ghalayini et al., 2018; Kartveit et al., 2019) and deep canyons along the Levant Margin (Druckman et al., 1995), which cumulated in a deep basin depositional environment from Oligocene to Early Middle Miocene times. Towards the end of the Miocene (within the Messinian), the closure of the Gibraltar Strait isolated the Mediterranean Sea from the Atlantic, resulting in the deposition of an approximately 2-km-thick multilayered evaporitic sequence across most of the Levant Basin until the re-establishment of a marine connection to the Atlantic (Haq et al., 2020 and references therein). At the terminal stage of the MSC, a seismically detectable unit is regarded as the latest expression of Messinian deposits in the Levant Basin and is named the Nahr Menashe deposits (Madof et al., 2019). This unit preludes a progressive return to normal marine conditions again.

Across the Levant basin, Feng et al. (2016) divided the Messinian evaporites into six Intra-Messinian seismic units (from deep to shallow) named ME1, ME2, MC1, ME3, MC2 and ME4 (Figure 2), which correspond to units 1–6 described by Netzeband et al. (2006), Bertoni and Cartwright (2007) and Gvirtzman et al. (2013). These seismic units are stratigraphically confined by the base of the salt or BS (Lofi et al., 2011) and the Intra-Messinian Truncation Surface (IMTS) by Gvirtzman et al. (2017) and Karveit et al. (2019), called also TES or TS (Feng et al., 2016; Lofi et al., 2011), and could also be correlated with the traditional M reflection (Ryan et al., 1973; Vidal et al., 2000). The extent of the IMTS in the Eastern Mediterranean has been widely mapped and observed in the Cyprus, Latakia and Levantine basins (Bertoni & Cartwright, 2007; Feng et al., 2016; Gvirtzman et al., 2017; Haq et al., 2020; Kartveit et al., 2019; Kirkham et al., 2020). This truncation surface has been variously interpreted as a product of subaerial exposure and erosion linked to relative sea-level fall (Bertoni & Cartwright, 2007; Kartveit et al., 2019), combined with a tectonic shortening related to the Cyprus Arc subduction (Maillard et al., 2011), or due to dissolution process as a result of freshening of the water column and the development of a stratified deep water basin (Gvirtzman et al., 2017). Recently, Kirkham et al. (2020) proposed an alternative model where the IMTS truncation is interpreted as the result of a major phase of syn-Messinian deformation that uplifted the salt progressively across the thermocline and into the thermally undersaturated epilimnion where it was dissolved.

During Plio-Quaternary times, 1.5 km of fine-grained siliciclastic sediment was deposited over the evaporites (Kartveit et al., 2018). Sediment was sourced from both the Nile delta (Niyazi et al., 2018, Zucker et al., 2021) and the Levant basin margin (Gardosh et al., 2010) with a basinward progradation (Lazar et al., 2016) observed across all the Levantine area. From a structural viewpoint, the interplay between differential sediment loading (Netzeband et al., 2006), inland uplift (Gvirtzman et al., 2013) and basin tilting (Cartwright & Jackson, 2008; Gradmann et al., 2005) affected post-Messinian deposits by triggering salt movement (Evans & Jackson, 2019; Oppo et al., 2020) and slope instability as indicated by episodic submarine mass wasting (Frey-Martinez et al., 2006; Gvirtzman et al., 2015; Kartveit et al., 2018). On a regional scale, the north-eastern Mediterranean was also subject to collisional tectonics (Ghalayini et al., 2014; Hawie et al., 2013) producing crustal shortening along the basin margin and accretionary loading in the south (Maillard et al., 2011). The major extensional faults affecting the post-evaporitic deepwater deposits nucleate from the mobile salt and appear to be halokinetically generated rather than

recording a regional tectonic compressive event (Evans & Jackson, 2019; Oppo et al., 2020) suggesting that the intra-salt layer movement was initiated just after the deposition of Pliocene sediments (Gvirtzman et al., 2013).

3 | DATA AND METHODOLOGY

Approximately 3067 km^2 of merged Post-Stack Time Migrated 3D seismic cubes and six 2D seismic lines from Petroleum Geo-Services (PGS) acquired and processed between 2006 and 2013 were used in this work across the northern Levant Basin (Figure 1b). All data were acquired and reprocessed through time with the same acquisition parameters as a part of the Lebanon MC 3D project. The final stack data are represented as zero-phased data and displayed with SEG reversed polarity (Brown, 2004). On the seismic sections, hard kick reflectors show a downward increase in acoustic impedance and are represented by a red colour (trough) while a black colour (peak) is associated with a relatively soft event indicating a downward decrease in impedance. As in the Lebanon offshore basin, there are no publicly released well data-to-date, stratigraphic correlations (including their nomenclatures) of the different units based on previous studies (Ben Moshe et al., 2020; Cartwright & Jackson, 2008; Gardosh & Druckman, 2005; Gradmann et al., 2005; Gvirtzman et al., 2013; Hawie et al., 2013; Netzeband et al., 2006). Bin dimensions were 25 × 25 m during data processing. The dominant frequency (F) of the section of interest (below the seabed) ranges between 0 and 50 Hz. The dominant frequencies of seismic data are 50 Hz in the post-salt overburden, 25 Hz in the Messinian evaporites and 17 Hz in the sub-salt units. Average P-wave velocities for these intervals (2000, 4200 and 3000 m/s, respectively) are derived using information from exploration wells in the southern Levant Basin (Feng et al., 2016; Gardosh & Tannenbaum, 2014) and data-processing reports by PGS Geophysical AS. Using the end-member velocities and frequencies, we estimate a vertical resolution (defined as tuning thickness, $\lambda/4 = v/4F$, being) of 10, 42 and 44 m, respectively. Gvirtzman et al. (2013) suggest a velocity of 3600–4000 m/s for the top of unit 6 in our paper showing a dominant frequency of 45 Hz.

In this study, the base of Messinian Salt (BS), the Base of the Nahr Menashe (BNM), Top of the Nahr Menashe (TNM) and Sea Bed surfaces have been mapped (Figure 3a–c) using initially a 10 × 10 inline and crossline increment (equivalent to a 125 × 125 m grid) then interpolated using converging interpolation algorithm down to a single inline and crossline spacing. Within the NMU more focused surfaces have been instead mapped using a 1 × 1 mapping increment (25 × 25 m). Considering the focusing effect of Kirchhoff migration (Brown, 2004), the horizontal resolution on the seabed mapped surface can be considered equivalent to the line spacing (Lebedeva-Ivanova et al., 2018).

In this paper, we interpreted the seismic data to map key stratigraphic horizons: top salt (TS) and base NMU, top NMU and the first package draping above it. Thickness surfaces have been derived for both the NMU and the post-NMU package unit above. Post-stack seismic attributes Variance (Chopra & Marfurt, 2007) and Root Mean Square (RMS) amplitude have been calculated (Barnes, 2016). Frequency decomposition and an RGB blended view of three selected frequency spectra (Henderson et al., 2008) using GeoTeric have been used to highlight channel and valley features. Frequency decompositions were generated by extracting a single power spectrum from different time slices across the target zone. The time slice was flattened in order to reduce the base salt intrusion deformation perturbating the image. Using these power spectra as a guide, constant Q decomposition bands with low (20 Hz), medium (30 Hz) and high central frequencies (40 Hz) were chosen to

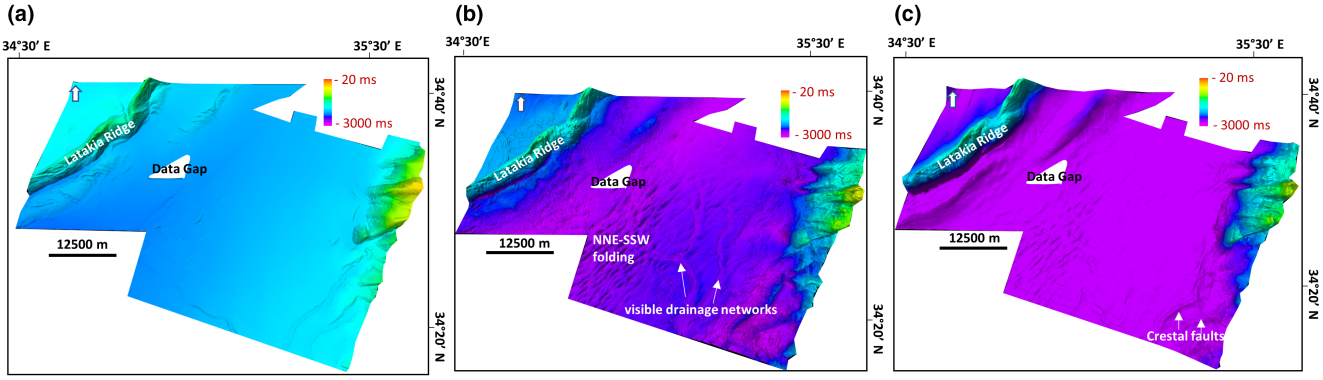

FIGURE 3 Time–structure maps of three prominent seismic markers in the Levant Basin. (a) Sea bed, (b) BNM or IMTS, this is the surface that has imprinted dissolution features, impression of drainage systems and NNE–SSW anticlines and (c) Base of Evaporites.

fit within the extracted spectra (Jilinski & Wooltorton, 2016). RGB colour blends were then generated by assigning red, green and blue to the equally scaled 20, 30 and 40 Hz magnitude volumes. Finally, a qualitative seismic facies analysis approach using the character of a group of reflections involving amplitude, abundance, continuity and configuration of reflections has been applied with the aim of characterizing the seismic facies response of the NMU.

4 | RESULTS: NAHR MENASHE DEPOSITS IN THE LEVANT BASIN

The uppermost deposits of the Messinian evaporites in the north-eastern Levant basin are bounded by two seismic reflectors both characterized by hard kicks. The Top of the Nahr Menashe is here called the Top Nahr Menashe (TNM), while the base of this unit is referred to as the Base Nahar Menashe (BNM) which chiefly corresponds to the Intra-Messinian Truncation Surface—IMTS (Gvirtzman et al., 2017). The thickness of the NMU varies to a maximum of 180 ms (twt) on the southern and deepest part of the basin, thinning to the single reflector resolution (the top and bottom reflectors now merging) along the shelf-slope area of the basin (Figure 4). Within the NMU, we can observe variable frequencies of internal reflections having moderate to strong amplitudes. Some repetitive (maximum 2–3 cycle), coherent, strong amplitude and semi-continuous seismic packages are observed in the southern and central part of the deep basin although numerous erosive features and post-depositional faults and folds have extensively modified their internal reflections. The internal seismic expression (strong amplitude, high frequency and semi-continuous) of the NMU has a strong similarity to the intra-halite reflectors interpreted as clastic units by Feng et al. (2016) (across units 4–6 of the MU—see Figure 2) rather than the overlying deepwater Plio-Quaternary sequences (Kartveit et al., 2018) and will be described later in detail. The BNM is affected by NNE–SSW trending compressional folds (Figure 3b) that are up to 18 km long and 3 km wide both in the northwestern and in the southern central part of the data set as also noted initially by Ghalayini et al. (2014) and subsequently by Madof et al. (2019).

4.1 | Top surface of Nahr Menashe (TNM)

In the northern Levant Basin, detailed mapping of the TNM produces a surface characterized by erosive channel/valley features which merge southwards to create an overall north-to-south-directed drainage network with intervening residual highs (Figure 5). The principal erosive structures have widths from 1 to 3 km and depths of 10s to 100 s of meters (maximum 60 ms twt) and are referred to as seismic valley features (Figure 4). Detailed mapping of these structures shows that the largest valleys comprise a series of nested erosional features that appear to stack laterally to form a composite basal erosional surface (Figure 6b). In the northwest of the study area, the drainage network is characterized by smaller erosional features (channels) that have a width of a few 100 m and form a well-developed tributary drainage pattern up to 50 km wide which extends for up to 500 km along a north-east to the southwest direction (Figure 4).

The principal valley-type features run close to parallel to the Levant margin. In places, erosional drainage networks are modified by subsequent salt movement (Figure 6a,b). Salt structures can be imaged through semblance image analysis or spectral decomposition (Figure 5b), which show that the salt reshapes or perturbates the main channel system geometry (Figure 5b, white arrows).

A detailed analysis of the TNM reflector indicates that the top surface of this unit is not always defined by a distinctive single reflector but often by composite erosive reflectors (Figure 6b,c).

4.2 | Basal surface of Nahr Menashe (BNM)

The BNM reflector is characterized by a hard kick and appears very well preserved, remarkably smooth and displays a more continuous reflectivity than the TNM. Overall, the surface appears mostly conformable except where it has been modified by the post-depositional salt movement to produce contractional symmetric and asymmetric folds (Figure 6a,b) of 50–150 ms (twt) dimension or it truncates the deformed salt structures (Figure 9b). The basal surface does not appear to be affected by the incised valleys or incisional drainage networks affecting the NMU (Figure 6a–c). The mapped BNM surface displays scattered circular and semicircular depressions that often appear as isolated linear expressions eroding this surface (Figures 7–9) and are described in detail below.

4.2.1 | Circular depression type seismic features

Numerous circular, semicircular to elongate, randomly distributed depressions are observed affecting the BNM

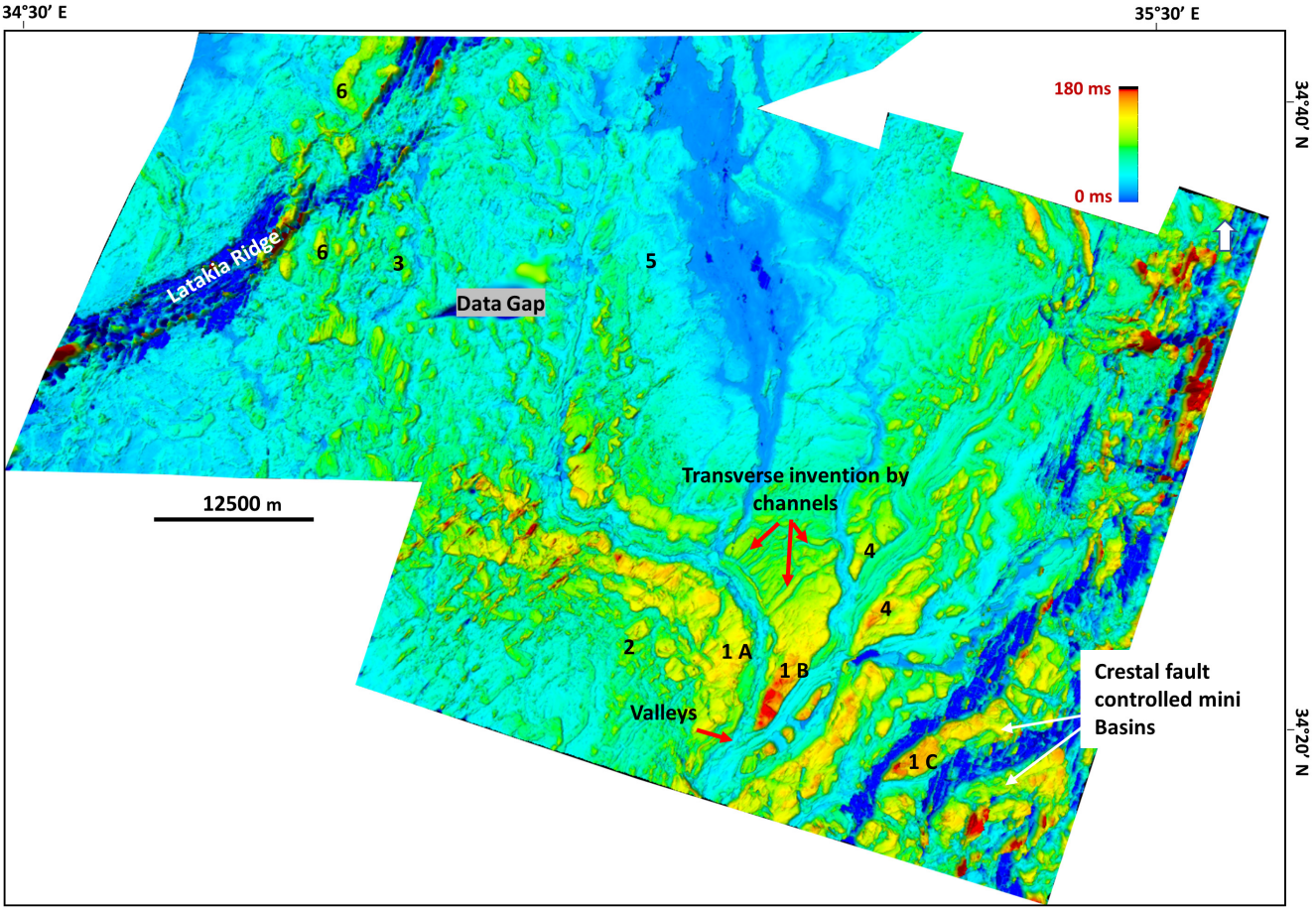

FIGURE 4 Thickness map (twt) of the Nahr Menashe Unit in north-east Levant Basin illustrates the distribution of the remnant blocks after dissolution and fluvial incision over this unit, numerous channels also invaded the top unit transversely.**Numerical values indicating the interpreted seismic facies distribution within Narh Menashe (Figure 14).

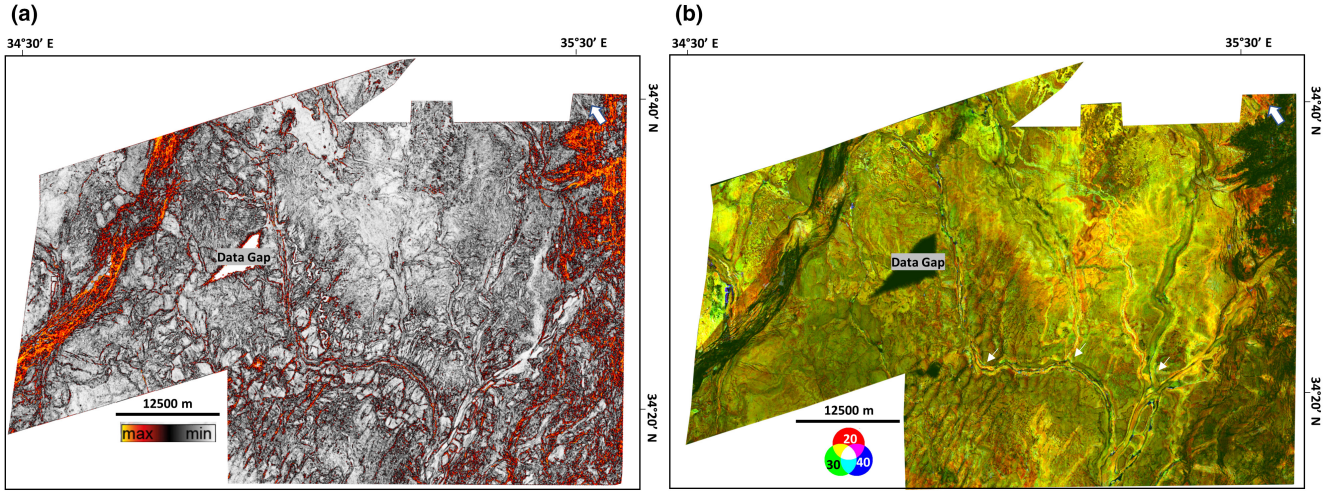

FIGURE 5 Attributes maps (time slice) on Nahr Menashe Unit showing the morphology and distribution of channel/valley systems over the unit. *Bottom of this Unit (BNM/IMTS)* has been flattened for better understanding.

surface. The depressions are 50–700 m in diameter, up to a maximum of 60 ms (twt) in depth, occasionally clustered or isolated, and often bordered by linear erosive features (Figure 7). The BNM surface shows a hard kick reflection response. Examination of the seismic reflections defining the deposits filling the circular features indicates that the

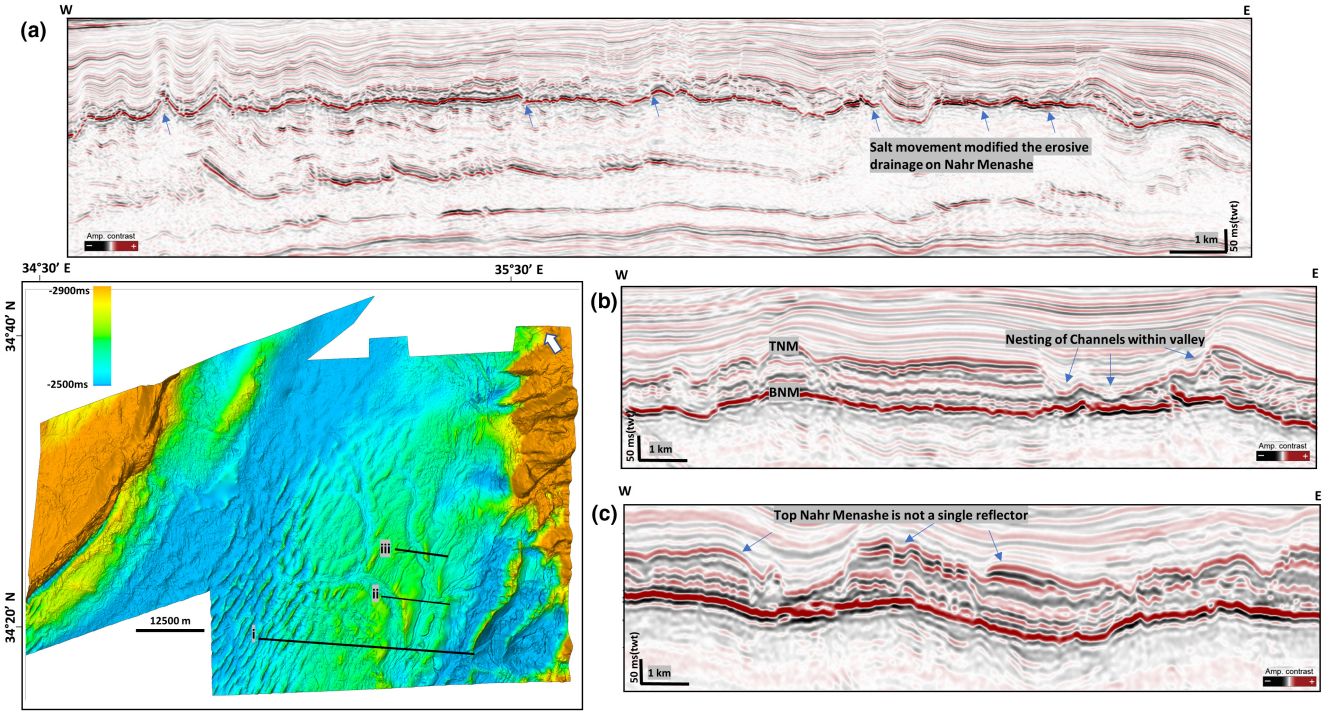

FIGURE 6 Surface map of the Nahr Menashe Unit indicates drainage systems that invaded through this unit, seismic profiles i, ii and iii illustrate the distribution of Nahr Menashe and its interaction with the fluvial incision and erosion. (ii) Illustrates the nesting of channels within the valley, (iii) Has been marked with blue arrows how the TNM has been eroded as it is not a continuous reflector rather varies with Top Messinian Units remnants.

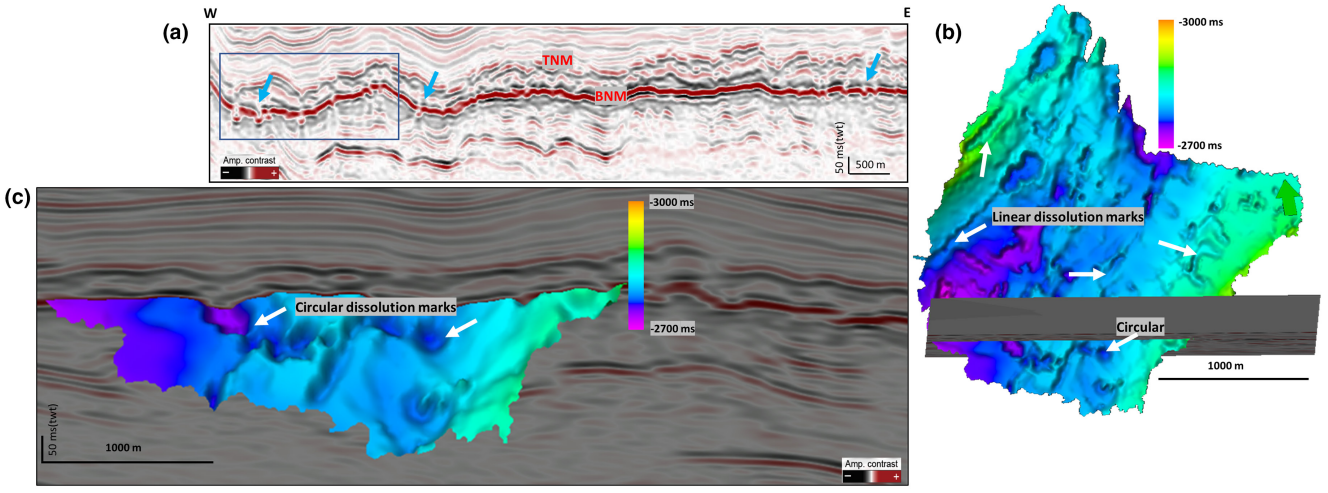

FIGURE 7 (a) An east west random profile showing depressions or dissolution imprints on BNM, blue rectangular part on the seismic section has zoomed and mapped, (b) Circular and linear dissolution imprints on BNM, material draping onto the accommodation spaces, no channel or erosive valley related to it, ▭ and (c) Circular and linear dissolution features are randomly distributed on BNM surface and they are not interrelated.

material drapes or has slumped into the depression and is defined by soft materials (with soft kick response). The features observed are suggestive of dissolution and collapse mechanisms associated with underlying salt bodies followed by a draping and/or passive collapse of material into dissolution hollows. Similar structures have also been described across the equivalent IMTS regional erosive surface in offshore Israel by Cartwright et al. (2012) and were interpreted as being generated by salt dissolution. Significantly, the distribution of dissolution features does not show any relationship with the drainage network described above on the TNM (Figure 9a,b).

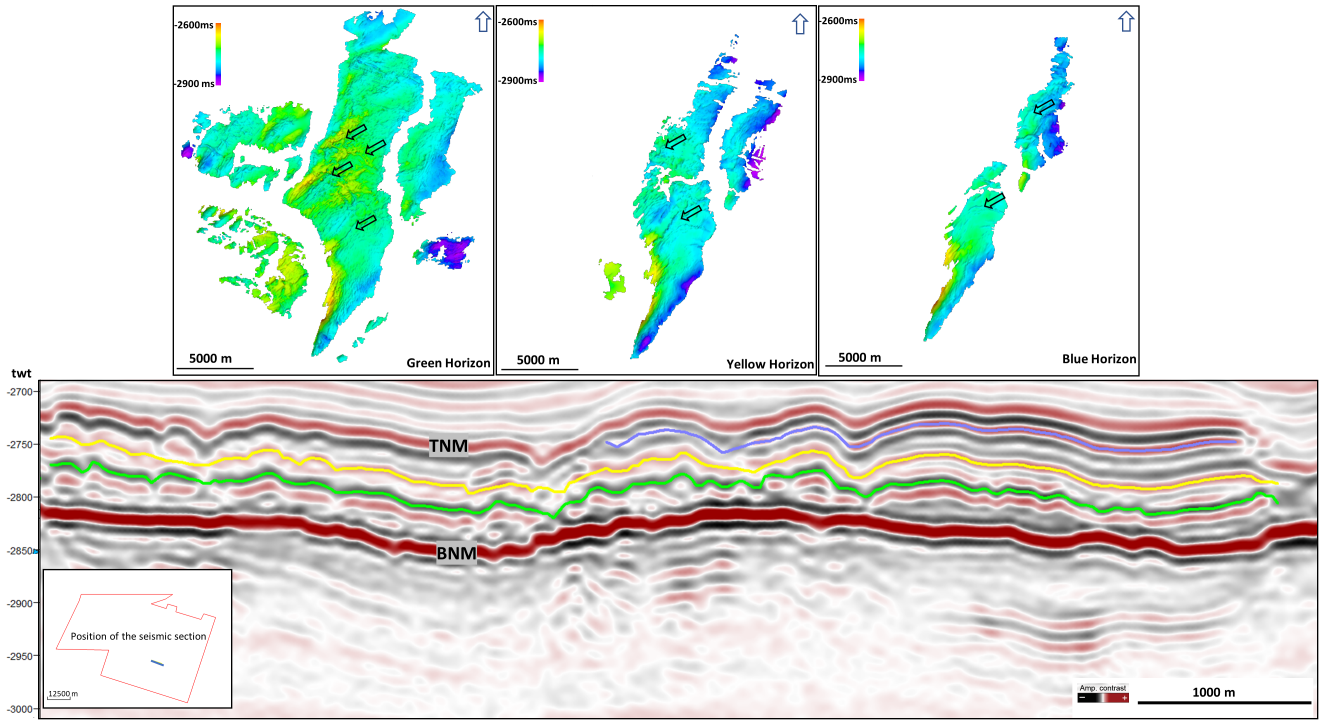

FIGURE 8 Time structure maps of Intra-Nahr Menashe reflections, every surface has the signature of intense dissolution (random linear imprints, circular depression), similar to Intra-Messinian Truncation Surface (BNM surface).

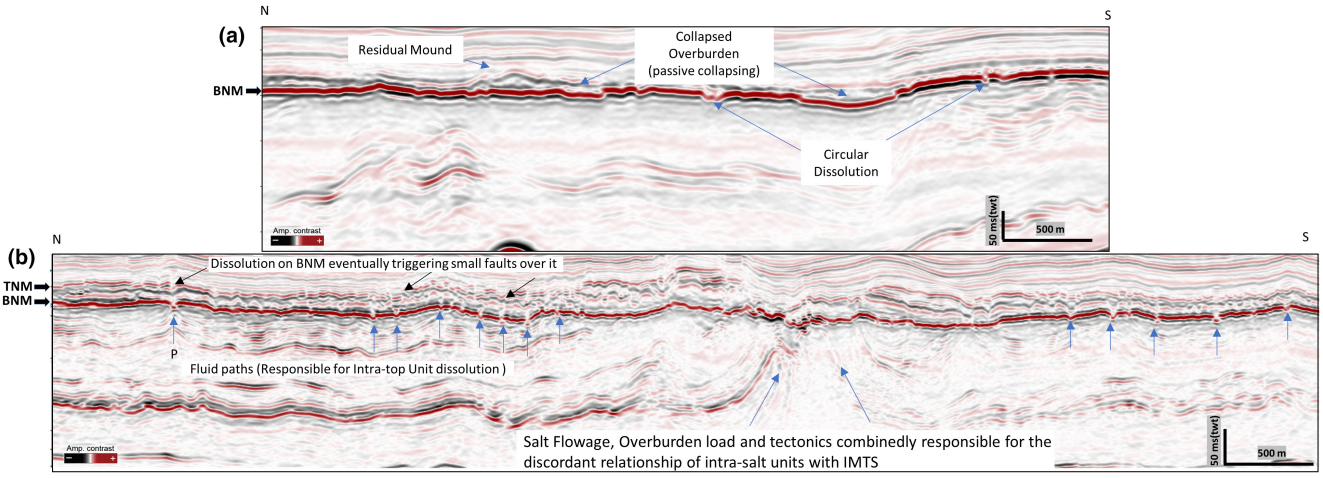

FIGURE 9 Seismic signatures of the dissolution features affecting the BNM surface. (a) circular depression, collapsed overburden (passive collapsing), residual mound on BNM surface (b) blue arrows indicate the broken nature of BNM, P marked as the effect of fluid migration from below. Extensive dissolution on BNM eventually triggered some small faulting (intra-NMU faulting).

4.2.2 | Linear depression type seismic features

Linear depression features 100–5000 m in length, 20–80 m wide and up to a maximum of 20 ms (twt) in depth which initiate and terminate abruptly (truncating underlying reflectors) are systematically observed and mapped across the BNM (Figure 7) and within the internal reflectors of the NMU (Figure 8). These linear depression features imprinted on the basal surface and intra-Nahr Menashe reflections do not show any preferred orientation (Figures 7 and 8). In some cases, in cross-sections, these features appear as small collapse structures underpinned by bright anomalies or affected by small pipe structures (see blue arrows in Figure 7).

4.2.3 | Collapsed surface or passive collapsing of BNM

The linear features described above may form zones of weakness along erosional or what appear as dissolution features which in places are further exploited by faults leading to collapse structures (black arrow, Figure 9). These passive fault collapse features are 150–800 m long, a few 10 s of metres in width, and 30–50 ms (twt) deep (Figure 9). The collapse of the BNM also affects the overlying NMU which tends to passively infill into the underlying area. This dissolution process has been ascribed by different authors to overburden deformation (Cartwright et al., 2001; Jackson et al., 1994; Jackson & Hudec, 2017) intra-layer faulting (small scale), fracturing or cave collapse (Zeng et al., 2011).

4.2.4 | Fluid leakage and vertical dissolution features

Flanking the dissolution features and the collapsed areas of the BNM reflector, we observe, vertical or sub-vertical pipe-like structures that initiate from the BNM and cross through the NMU producing a clear downward deflected v-shaped depression that dies out downwards (Figure 9b, blue arrow). These features are up to 120 ms (twt) high and 50–90 m wide. They are distinctive from the circular and linear dissolution features observed along the BNM and the intra-layer of the NMU. We interpret these features to form as a result of the interplay between dissolution mechanisms from fluid percolating and fracture nucleation that exploits collapse structures produced by the salt movement. Dewatering of the top salt unit could produce fluid migration along fractures affecting the TNM (Figure 9b). In other places, the fractures are filled with insoluble materials that infill through collapse from above (Figure 9b). Similar discordant pipe-like structures are also documented in the salt unit of the Santos Basin, Brazil (Rodriguez et al., 2018), the Fort Worth Basin (carbonate rocks), Texas (Hardage et al., 1996) and the Persian Gulf (Burberry et al., 2016) where they are similarly interpreted as dissolution-related leakage pipe breccias.

Some vertical dissolutions features displaying pipe-like structure (marked as P in Figure 9b) can be traced down into the lower evaporite units. Similar cross-evaporite fluid flow, as indicated by the presence of pockmarks and gas chimneys, has been described across the Levant basin (Bertoni & Cartwright, 2015; Bowman, 2011; Oppo et al., 2021). Numerous vertical fractures that are present throughout the NMU are associated with small intra-layer faulting in some areas and together with the broken nature of the bottom reflector of this unit further suggest that upwards brine migration occurred from below the NMU. The diagenetic transition of gypsum to anhydrite (carnallite—sylvite also) may result in the generation of brines in the subsurface and may also provide the force required to generate fracturing (Bertoni & Cartwright, 2015).

4.3 | Top Nahr Menashe and post-Messinian Units

The first laterally continuous marker horizon (pink reflector in Figure 10) referred to as the top marker horizon that can be mapped above the NMU, appears as a reflection boundary showing a mappable continuity and internal coherency. This surface can be mapped across the entire study area above the TNM except in places affected by recent structural features such as the Lebanon Fracture system, Latakia Ridge and crestal faults. The package between the TNM and the top marker defines a seismic package that is finely layered internally. The complex drainage patterns that incise the NMU appear passively infilled as indicated by reflectors that drape or onlap the valley margins (Figure 10a–c). Truncation or termination

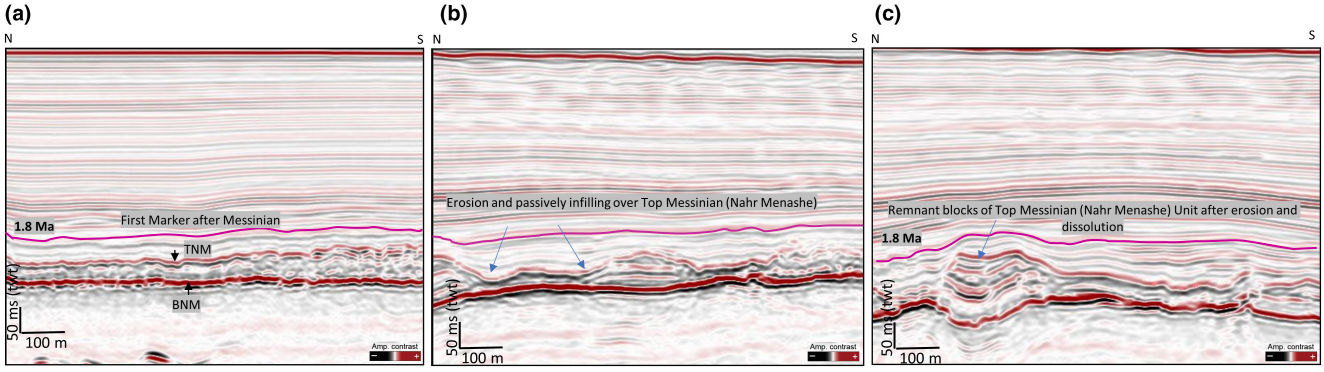

FIGURE 10 The interpreted pink reflection is considered to represent the first regional post-Messinian marker that can be mapped throughout the study. It separates overlying marine Plio-Quarternary sequences from the underlying transitional units (infilling).

of the underlying reflections of this package against the top marker horizon (pink horizon) indicates that this horizon represents at least in part, an erosional surface (Figure 11). The top marker horizon (pink reflector) is also conformable with overlying reflections interpreted to represent deepwater deposits (Figures 10 and 11). The thickness map of this package (between the TNM and the top pink marker) shows the clear infilling character of the package (Figure 12). The map shows the average twt thickness of the TNM-top marker unit varies between 40 and 160 ms across the basin, with maxima in the deepest valley fill section in the central-southern part of the study area (Figure 12). The package is stratigraphically lower than the regional 1.8 Ma horizon interpolated using the information by Kirkham et al. (2020). The camparative RMS amplitude distribution maps (Figure 13) provide some clues about the drainage systems and infilling lithologies, within Nahr Menashe the drainage filling has higher RMS values (Figure 13a) pointing to different lithologies than the host (potentially coarser than the Nahr Menashe). Whereas the infilling has lower RMS values than the surrounding within the packages above the Nahr Menashe (potentially finer than the surrounding).

5 | SEISMIC FACIES WITHIN THE NAHR MENASHE

Detailed seismic and attribute mapping of the Top Messinian Unit across offshore Lebanon, including the platform to the deeper part of the north-eastern Levant basin, has allowed the recognition of several internal seismic facies characterizing the NMU. Six distinctive seismic facies (Table 1) have been identified and categorized based on a seismic facies approach, that is internal reflection continuity, amplitude, thickness and coherency. The facies suggest a strong lateral variation in the internal character of the top unit. All facies are affected by

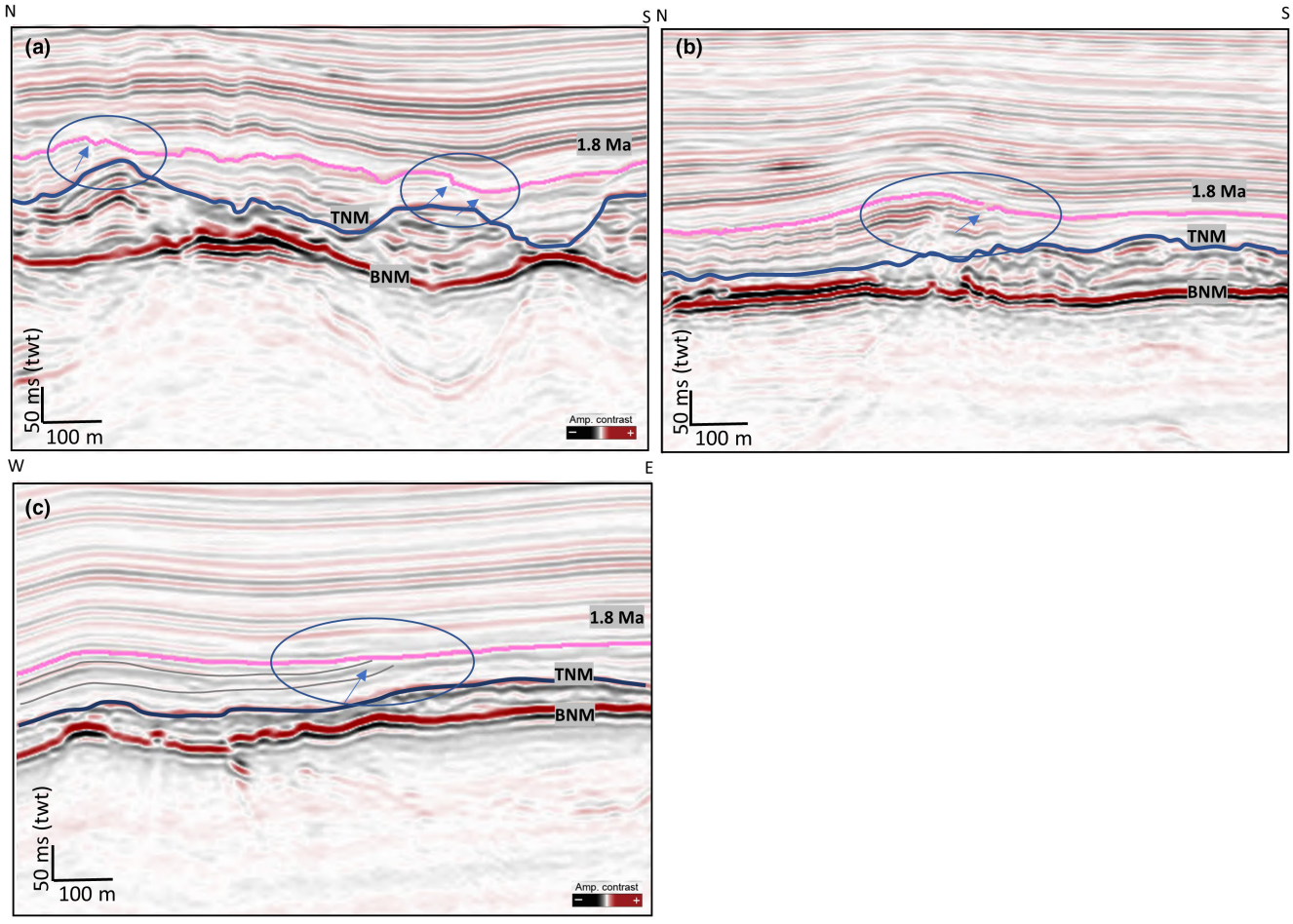

FIGURE 11 The pink seismic event represents an erosional surface in places as shown by lower reflections being truncated beneath it. See arrows marked in a–c. Notice also the reflection characteristics of the seismic units below the package bounded by the pink reflector (discontinuous, broken, low amplitudes and moderate frequency) and above it (continuous, mappable, moderate to high amplitude and coherent).

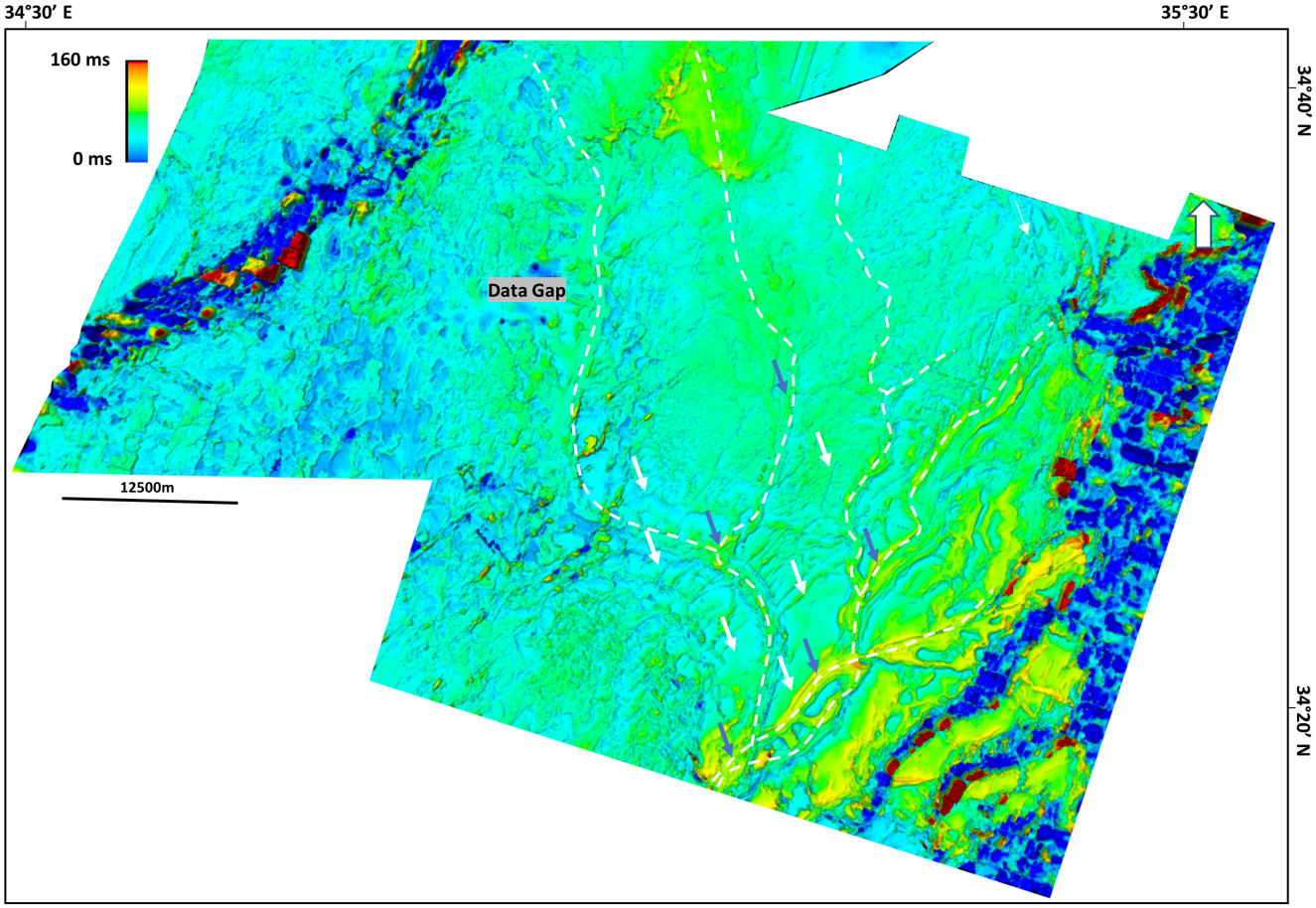

FIGURE 12 Thickness map (twt) between Top Nahr Menashe and Marine Marker. Blue arrows indicate valley or channel filling after marine transgression and white arrows indicate low thickness due to remnants (blocks) of Nahr Menashe, dotted white lines are axes of the paleo drainage network over Nahr Menashe, sediment thickness is more over the base of erosional drainage network rather sides.

fracturing, faulting and different amounts of dissolution related to the latest deformation/salt tectonic event (Oppo et al., 2020).

5.1 | Seismic facies 1

This facies comprises two of three cycles (cycle here defined as a peak-through-peak triplet) of coherent seismic packages characterized by parallel, internal, semi-continuous to continuous reflections showing strong reflectivity (Figure 14). This seismic pattern has been mapped as a 120–180 ms (twt) thick package, 0.5–3 km in length, and is frequently fractured and contains intra-layer faulting. This facies is observed only where the NMU is at its thickest and adjacent to the erosive valley walls. Internal reflections of the coherent packages are often truncated by high-angle valley walls (apparently dipping up to 45° in some places, Figure 14, feature 1A). From a seismic textural viewpoint (geometrical internal character of the facies), the reflection pattern (strong amplitude and frequency) has a close resemblance to the underlying clastic part of the Messinian salt and is distinctly different from the overlying Plio-Quaternary high-frequency low reflection pattern (Figures 15 and 16). Within this facies, we recognize three different post-depositional modification subclasses with external sheet geometries (Figure 14, feature 1A):

Subclass 1A conformably overlies the BNM where internal reflections are defined by strong cyclic and continuous reflections that are mostly undeformed (no intense fracturing, faulting or collapse). To investigate the seismic morphology of the continuous reflectors, three horizons were mapped in detail (Figure 8). Each horizon (Figure 8) displays features characteristic of dissolution such as linear, semicircular depressions (white arrow in Figure 8) which occasionally terminate against faults and internal fractures and are strikingly similar to the morphological features observed on the BNM. In most cases, faults/fractures die out within this package (Figure 16) suggesting this package defined by subclass facies 1A has a brittle behaviour. These linear dissolution marks 150–400 m wide and 500–5000 m in length

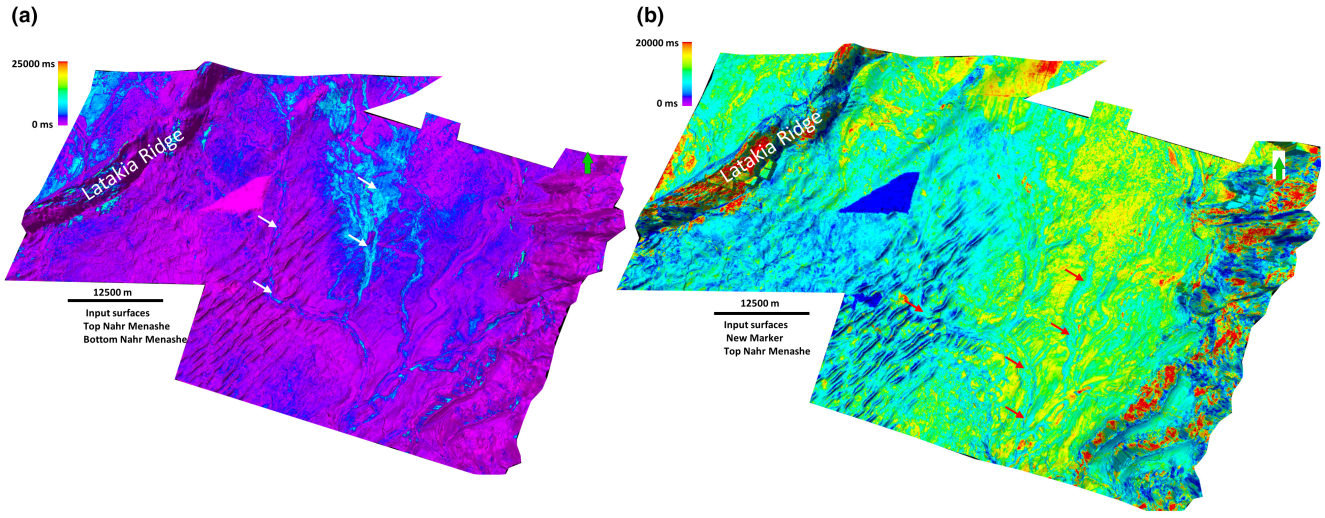

FIGURE 13 RMS amplitude maps of (a) Nahr Menashe, white arrows indicate higher amplitudes inside the drainage net network from surroundings, and (b) Marine Transgression Deposits, red arrows indicate lower amplitudes inside the drainage net network from surroundings.

are mapped within intra-layers and decrease in intensity and number upwards (bottom to top horizons). Some of these features observed in the BNM (Figure 7a) are linked to small vertical features which do not cut the entire NMU and show amplitude anomalies suggesting fluid movement from lower salt units through the BNM. On the surface, they coincide with circular or linear erosive marks, with no displacement, which are here interpreted as resulting from post-depositional diagenetic changes due to the movement of undersaturated brines from lower salt units through the BNM, coupled with internal deformation associated with intra-formational gravity gliding.

Subclass 1B is also characterized by coherent cyclic seismic packages but is affected by strong fracturing and intense faulting crossing the NMU (Figure 14, see seismic feature 1B). The BNM below this subclass appears broken, collapsed or faulted and associated with cross stratal fluid/brine migration discussed for subclass 1A.

The third subclass of the coherent cyclic packages is characterized by a seismic package that displays discontinuous reflections, affected by crestal faults and bordered by dip slopes controlled by salt intrusion (Figure 14, see seismic feature 1C). They represent the equivalent of facies 1A and 1B but are strongly deformed by the salt intrusion.

5.2 | Seismic facies 2

This mounded seismic facies is characterized by a strongly eroded and reworked package where a soft kick is coupled to the hard kick that defines the base of the Nahr Menashe. The thin package appears chaotic at the top of the Nahr Menashe and shows subcircular elongate mound-shaped seismic features (Figure 14, see seismic feature 2).

5.3 | Seismic facies 3

In the south-western part of the study area, the NMU appears completely deformed, with both internal and external reflections affected by the combined effects of fluid escape, lower boundary collapse and intra-layer faulting and fracturing (Figure 14). Internal reflections are broken. Numerous u-/v-shaped channels further modify the top surface of this unit. The orientation of these channels appears unrelated to underlying salt structures (Figure 4) and are mapped in areas where the entire thickness of the entire halite unit is preserved. Occasionally, the internal reflections of the top part of this unit show a tendency for downlap to the BNM boundary are strongly deformed. The broken nature of internal reflections suggests the relatively brittle behaviour of the materials.

5.4 | Seismic facies 4

Seismic facies 4 has a smooth continuous top boundary but the internal reflections appear chaotic as the individual reflections/horizons cannot be traced. It is mapped in the central part of the study area where it is preserved in between erosive valley/channel networks affecting the TNM. This unit has a uniform thickness (~80 ms twt) with an undisturbed top boundary. The lower boundary displays collapsed features and the sediments from the upper part of the unit drape or fall into the available

TABLE 1 Seismic facies characteristics of the Nahr Menashe Unit and interpretation

Category	External shape and relationship to salt	Internal reflection characteristics	Occurrence	Interpretation
1A	Sheet, conformable to salt	Parallel, continuous, moderate to strong amplitudes, two of three coherent cycles	Bank of the valley/ channel system, salt triggered fold valleys	Remnant and undisturbed blocks, due to a more confined and incised valley system, interpreted as relic Islands
1B	Conformable to rugged, wedge	Parallel, moderate to strong, two of three coherent cycles, internally faulted	Traced on flanks of valleys and salt diapirs also in valley banks	Fractured and intra-layered faulted, clastic admixtures made internal layers more brittle, dissolution surface (lower boundary) also cracked or fractured
1C	Sheet	Mostly parallel, faulted/ fractured, strong reflectors, coherent (two of three cycles)	Present on dip slopes of tilted fault block crests	Crestal fault created mini basin, small channel seen on the consecutive fault breaking point
2	Mound, occasionally truncated with intra-salt stratigraphy	Semi-continuous, mound-shaped, moderate to weak reflection	South-western part of the valleys associated with sinkholes	Brecciated karst (salt/limestone), subaerially exposed at the very last stage, sinkhole and fluid pipe noticed on the lower boundary
3	Sheet, downlapped	Multi-cycle, no definitive internal reflection, the top boundary is difficult to trace	South-western part	Dissolution coupled with u-/v-shaped channels and fractured-internally faulted
4	Sheet, down lapped	Multi-cycle, no definitive internal reflection, top boundary is difficult to trace	Central northern part	Extensive dissolution process worked on the lower boundary, sediments from upper units drape of collapsed into the accommodation
5	Sheet drape	Without internal reflection, low amplitude	Towards NW	Fine-grained lithology with somewhat below seismic resolution
6	Mound, sub-parallel and following dips of intra-salt stratigraphy	Low to moderate amplitude, discontinuous, sub-parallel to wavy	Both sides of the Latakia Ridge	MTD followed Latakia slopes

accommodation spaces (Figure 14), see seismic feature 4, but also discontinuous and broken internal reflectors producing an overall chaotic pattern of the internal reflections within this facies.

5.5 | Seismic facies 5

Seismic facies 5 occurs in areas where the thickness between the TNM and BNM appears to be thin (sometimes below seismic resolution) and almost unaffected by deformation and is characterized by residual mound features that overlie vertical fractures breaching the BNM surface. This seismic facies has a sheet-like geometry with draping to pinch-out type stratigraphic signature (Figure 14), with gradual reduction in thickness of the NMU. In some specific places, the TNM merges with the BNM, and the internal reflections are difficult to distinguishable individually.

5.6 | Seismic facies 6

Along both the flanks of Latakia ridge and along the slope of the Lebanon basin margin where post-Messinian compressional fault re-activation is well expressed (Figure 4), the seismic units are characterized by seismic packages

that either form a series of blocks that preserve internally coherent reflection packages but are bounded by faults or, show areas with a chaotic pattern, where reworked/redeposited facies are present. Within the blocks, internal reflections approximately follow the dip direction of intra-salt stratigraphy (Figure 14). This seismic facies is distinctive from the previous one and is found systemically along the Latakia Ridge or basinward or along the flanks of folded structures.

6 | DISCUSSION

The magnitude and duration of the MSC event including the sea-level drawdown varied significantly throughout the Eastern Mediterranean where Messinian deposits record distinct tectonic and stratigraphic histories across different mini-basins (Butler et al., 1995; Haq et al., 2020; Roveri et al., 2014). In the north-eastern Levant Basin, we have analysed seismic reflection data to characterize the nature of the terminal stage of the Messinian salinity crisis. To place our observations into context and to interpret the nature of reflooding of the basin it is important to reconstruct the termination history of the MSC in the Levant Basin.

6.1 | Base of Nahr Menashe

Across the entire Levant Basin and the Eastern Mediterranean in general, the base of the NMU has been interpreted as an erosional surface because of its discordant nature (up-dip termination, as an erosional unconformity) and the relationship with NW dipping intra-evaporite layers (Bertoni & Cartwright, 2007; Kartveit et al., 2019; Ryan et al., 1973). In our mapping, it coincides with the IMTS. Using seismic and well data (Aphrodite-2, Myra-1, Sara-1) from offshore Israel (Southern Levant Basin), Gvirtzman et al. (2017) interpreted this surface as a truncation surface generated by subaqueous dissolution. They proposed a horizontal chemocline model (halite-saturated hypolimnion and undersaturated epilimnion) for stratified water column (Figure 4 of their paper), to explain the origin of this surface and referred to it as the IMTS. Recently, Kirkham et al. (2020) mapped the extensive truncation relationship of the Base of the NMU as the IMTS at the base of the MU in offshore Israel (map 1b from their paper), supporting the dissolution model and separating marginal and deep basin environments where thermocline diffusion was responsible for dissolving the top of the salt (Figure 7 of their paper).

In this paper, we note that the BNM represents the second strongest acoustic reflection after the sea bed (Figure 2b) and coincides with the IMTS, thus allowing precise, continuous mapping of the surface across the entire data set. In our study area, we do observe the intra-Nahr Menashe layers of the NMU towards the deepwater basin, which when undeformed appear roughly concordant with respect to the BNM, but appear discordant or truncated towards the margin or where NMU is deformed by faulting, and folding due to the ductile flowage of salt (Figures 15 and 16). The BNM mapped surface, in the deeper part of the basin, displays strong dissolution features filled by NMU (Figure 7), similar to those observed by Kirkham et al. (2020), indicating that dissolution processes had acted on this surface prior to deposition of the NMU. These observations suggest that a laterally heterogeneous model should be adopted for the interpretation of the BNM surface across the basin. In the deeper part of the basin, a subaqueous dissolution process controlled surface development while erosional processes prevailed along the basin margin and across other elevated parts of the Eastern Mediterranean such as the Herodotus and Eratosthenes seamounts and the Latakia Ridge (Kartveit et al., 2019). Also, from a regional perspective, at this stage of the Messinian Crisis, the sea level is likely to have been close to its lowest point (stage 2) due to isolation related to the Sicily gateway (Camerlenghi et al., 2019; Haq et al., 2020; Roveri et al., 2014) triggering extreme evaporation, extensive evaporite precipitation and which at a certain point exposed some parts of the basin margin to subaerial erosion. We suggest therefore that following the consensus model (Roveri et al., 2014) the BNM may represent the boundary between stage 2 and stage 3 of the Messinian salinity crisis when halite-saturated brines were transformed to gypsum-saturated brines and/or brackish Lago Mare conditions (Gvirtzman et al., 2017) which were deposited above the BNM (Hilton, 2001; Kartveit et al., 2019). In summary, the seismic geomorphic features displayed by the BNM suggest that the laterally heterogeneous nature of this surface is related to strong dissolution (Gvirtzman et al., 2017) coupled with marine regression, and subaerial erosion along basin margins (Bertoni & Cartwright, 2007), and wave erosion (Bache et al., 2012) on intra-basinal platforms (Micallef et al., 2019).

6.2 | Interpretation of the seismic facies in the NMU

With the upper part of Unit 7 (sensu Meilijson et al., 2019), the Nahr Menashe deposits (Madof et al., 2019) are considered to represent the terminal deposits of the MSC. In our data set, the NMU displays an extremely variable seismic expression and thickness, from a maximum thickness of ~180 ms (TWT), with 2/3 cycles of coherent

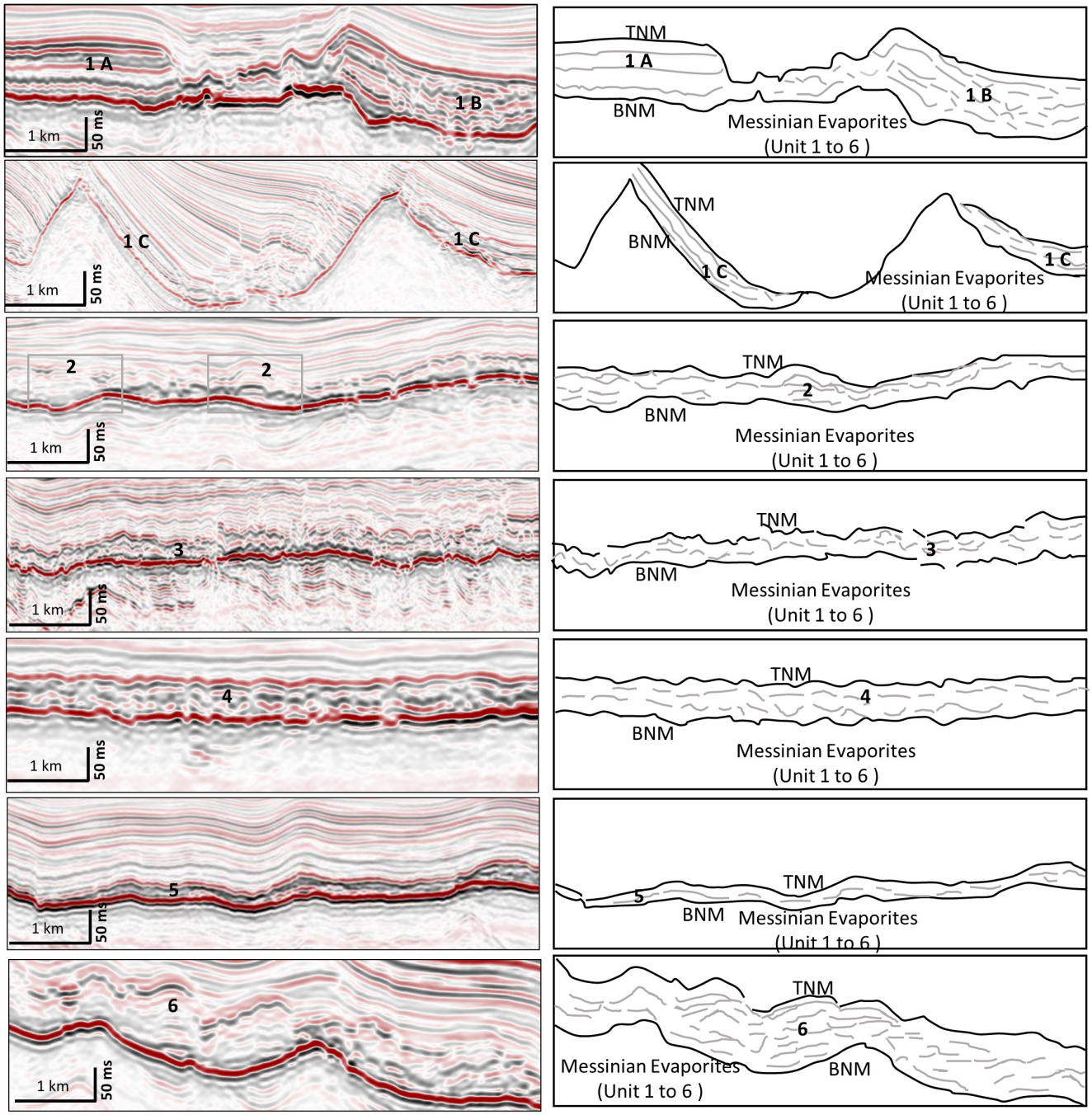

FIGURE 14 Seismic facies within the Top Messinian Unit (Nahr Menashe) in the north-eastern Levant Basin.

and strong seismic reflectors parallel to both top and bottom surfaces, to places where it shows evidence for strong dissolution at the base and within some layers. The seismic facies mapped across the NMU in the study area display a range of stratigraphic and structural characteristics that vary depending on the structural and depositional context within the Lebanon Basin (deep to marginal basin). In the deeper basin, where the NMU is better preserved (between erosive valleys) and unaffected by intrusive salt bodies, clear, distinctive strong cyclic and continuous reflections are present and mappable (Facies 1a). These are similar to the intra-salt reflection character described by Feng et al. (2016) and Gvirtzman et al. (2017) below the IMTS (here equivalent to BNM), suggesting that the Nahr Menashe stratigraphy likely represents a multi-layered system of thicker salt-evaporite units sandwiching thinner sand and shale units. In areas of salt movement, the NMU is deformed by well-defined faults and fractures that are confined within the unit (Facies 1b). In areas unaffected by the Curcular salt intrusion, or parts of the deeper basin, the NMU is thin or less layered (Facies 4 and 5).

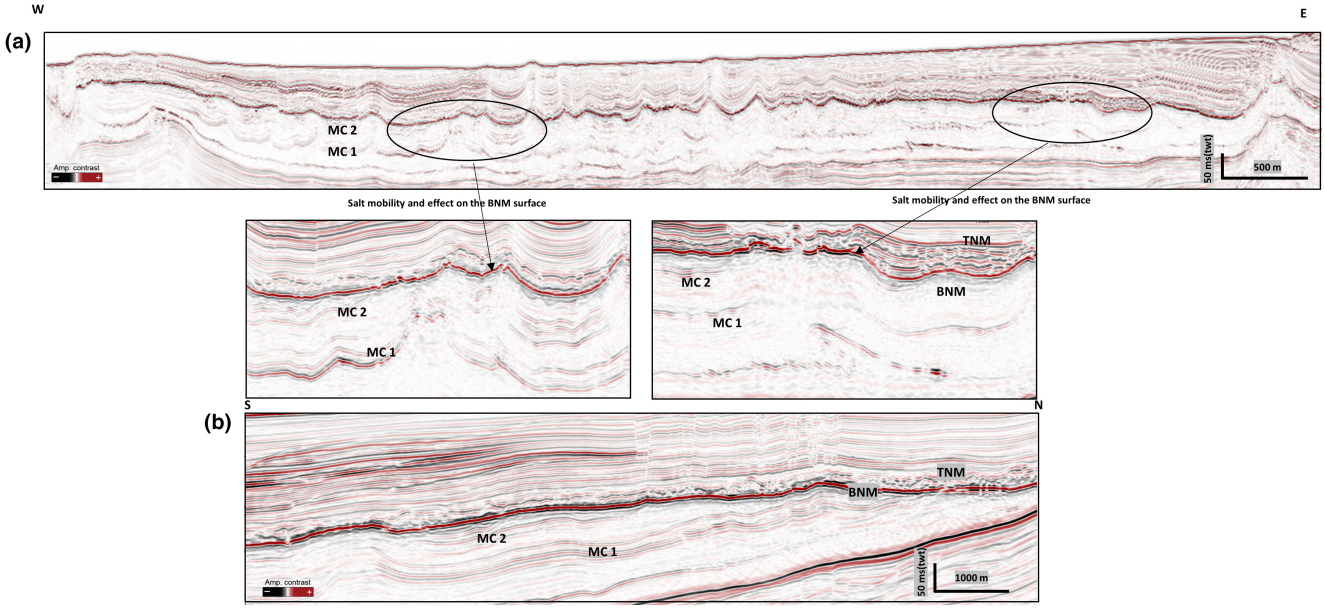

FIGURE 15 Random seismic profiles illustrate the perspective orientations of different intra-evaporite layers with BNM /IMTS, they are generally having a parallel relationship other than deformed by salt flowage, overburden load or tectonics.

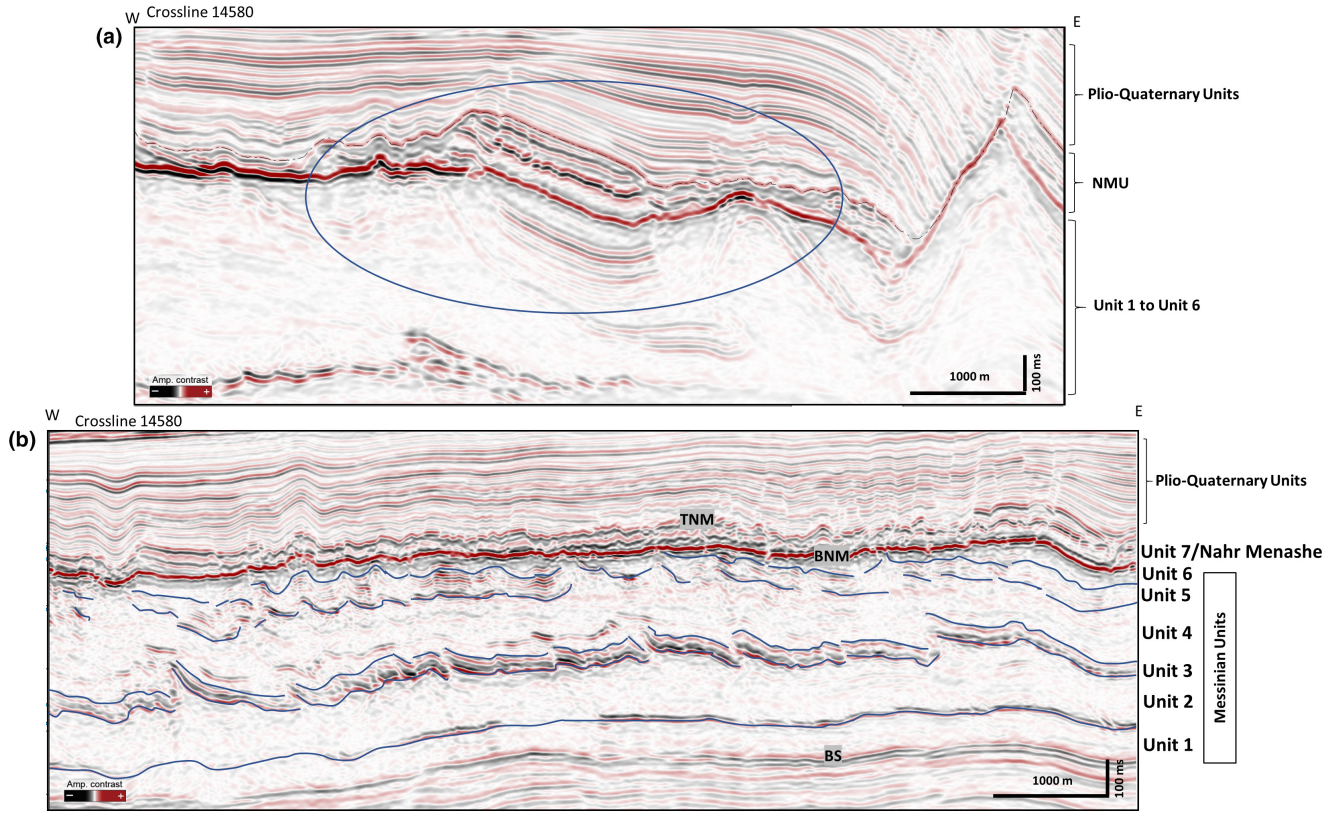

FIGURE 16 Nahr Menashe has a close resemblance with Messinian evaporite units rather above Plio-Quaternary marine sediments.

6.3 | Linear and circular dissolution structures

The entire NMU is affected by subcircular, elongate, mound-shaped (Facies 2) and linear seismic features. Where the NMU is well preserved and moderately deformed by salt flowage, dissolution features are observed and mapped systematically across both the BNM and each of the internal reflections. The linear feature in some cases mimic fractures but are much wider (50–80 m) and

their length varies from a few 100 m to several kilometres. They often appear and disappear without displacing reflectors. We interpret these to represent elongate and brecciated dissolution features and may represent karst (gypsum/limestone) generated by the removal of soluble salt (Jaworska & Nowak, 2013; Kyle & Posey, 1991) and residual less soluble parts that eventually became karstified. In the remnant area of the deep basin affected by salt intrusion or across the deformed shelf-slope area (Latakia Ridge and Levant fracture), collapse and crestal fault systems associated with salt dissolution affected the units across and above the NMU (Facies 1C and 6) making detailed reconstruction of the original stratigraphy difficult. Based on their seismic expression, geometry and scale, the subcircular- and mound-shaped features present both at the base and across the NMU appear closely similar to those documented by Rodriguez et al. (2018) in the intra-salt layer of the offshore Santos basin. They interpreted these features to represent sinkholes or dolines that formed due to evaporite dissolution at diapir crests. In contrast, the residual mounds form features 50–500 m in width with 10–50 ms height, often defined a by soft reflector that tops the base of the BMU (hard kick). All the seismic facies (Figures 10 and 11) affected by dissolution features are often characterized by poor internal stratigraphy and some part (south-western part of the study area) of the NMU unit has been strongly affected by after deposition compressive deformations events (e.g. Ghalayini et al., 2014; Hawie et al., 2013) making the clear characterization of their original internal stratigraphy difficult. Similar mound features have been interpreted from seismic data as the insoluble residuum left following the dissolution of halite-rich layers in deepwater settings (Jackson & Hudec, 2017). Similar features have also been described in the subareal realm by Stafford et al. (2008) and Chiesi et al. (2010) and interpreted as gypsum-dominated karst or residual mounds from areas strongly affected by near-surface dissolution. Large sinkholes observed by Gutiérrez and Lizaga (2016) on top of the crest of exposed salt domes in the Zagros mountains, an area currently affected by rapid subsurface salt dissolution, are of similar dimensions and geometries to the semicircular dissolution features we document here. During deposition of the NMU in the northern part of the Levant Basin, it is envisaged that complex shallow subsurface and subareal dissolution conditions related to successive rapid falling-regressive and rising-transgressive sea levels would have repeatedly affected the entire NMU. A similar interpretation is proposed also for the continental margin offshore Israel by Ben Moshe et al. (2020). They observe intense ravinement along a continuously regressing and transgressing coastline which exposed the slope gradient to subaerial processes generating channels as conduits for sediment bypass. During this regressive phase, the eroded strata (including evaporite materials from the Afiq unit) were evacuated downslope and deposited basinward of this depth. In our study area, during this regressive event, and persisting during the final erosive event producing the large canyon system, meteoric surface water seeped into NMU contributing to dissolving the evaporite components and enlarged fractures-producing karsts and dissolution structure within the top NMU surface.

6.4 | Interpretation of the TNM erosive features

Our 3D mapping highlights a complex drainage system characterized by numerous channel and valley features as first described by Madof et al. (2019), which incise the top of the unit but does not show erosion down to or below the basal surface (BNM) (Figures 10 and 11). The complex drainage appears passively infilled by a finely layered package of a different character, as suggested by the reflectors which appear to drape the valleys in the NMU. This observation suggests that the maximum base-level fall during late Messinian times did not drop below the BNM level and that erosion occurred after the deposition and/or redeposition of the Nahr Menashe deposits. The complex drainage pattern represents therefore the final erosive event of a more complex depositional history recorded by the NMU.

6.5 | Deformation of NMU

From a structural point of view, the NMU appears to have been affected by a post-depositional deformation event which triggered faults of various geometries and sizes. As described in facies 1C (Figure 14), some late faults are related to salt remobilized or intruding across the overburden as indicated by the crestal faults nucleating from the intrusive bodies and affecting the entire overburden (Oppo et al., 2020). Similar fault structures appear diffused around the Latakia Ridge, where the recent regional tectonic activity has overprinted earlier events (Ghalayini et al., 2014). In other cases, as shown by facies 6 (Figures 14 and 17), the NMU is affected by diffuse faults confined within the NMU, suggesting that the multi-layered package responded to salt deformation as an overall brittle or brittle–ductile unit. This indicates that the NMU is characterized by a complex internal mechanical stratigraphy compared with the upper Plio-Quaternary deposits. Kartveit et al. (2019) made similar observations and interpreted these small faults within the NMU as being controlled by anhydrite-rich layers.

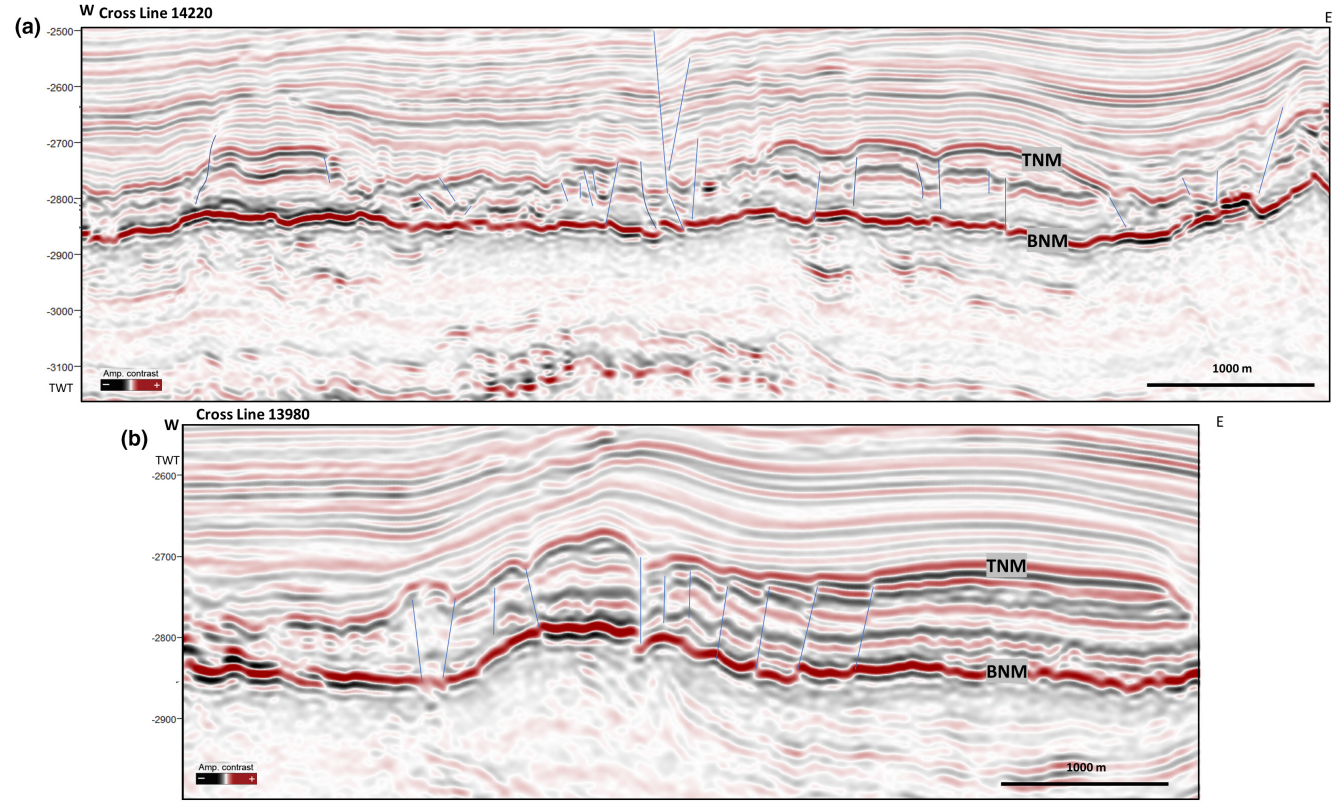

FIGURE 17 Numerous faults and fractures that originated and died within the Nahr Menashe Unit, signify more brittle materials within this unit than lower.

Gvirtzman et al. (2017) also re-constructed the lithology of Unit 7 across the Israel Levant basin using well log data including Gamma and Resistivity logs and pointed out the presence of alternating units of anhydrite, sand and clay layers, confirming the brittle–ductile nature of the Unit. Overall, the heterogeneity of the seismic facies, the internal erosive and dissolution features, and the multi-layered structural response to late deformation suggests that the NMU comprises a complex stratigraphy, including redeposited units observed along basin flanks or the margins of salt structures that deformed the NMU and punctuated by dissolution events.

6.6 | Salinity crisis events of north-eastern Levant Basin

Around 5.97 Ma evaporite (halite) started to precipitate from hypersaline seawater in the deep Levant Basin (Manzi et al., 2013; Meilijson et al., 2019). Marine conditions indicate that the western Mediterranean was connected to the Atlantic with open water exchange between the eastern and the western Mediterranean Basins through the Sicily getaway (Güneş et al., 2018; Haq et al., 2020). Isolation of the western Mediterranean from the Atlantic and Eastern Mediterranean by the Sicily gateway (Camerlenghi et al., 2019; Güneş et al., 2018), eventually led to the accumulation of multi-cycle evaporites (Gvirtzman et al., 2017) in the deep Levant Basin. This step corresponds to the latter part of stage 1 and stage 2 of the MSC (Meilijson et al., 2019). Gradually, the Northern Levant Basin became a marginal marine basin due to the continuous precipitation of salt and lowering of sea level. Marginal basin areas were subject to subaerial exposure due to either lowering of sea level or isostatic forces as proposed by Kirkham et al. (2020) (Figure 7 of their paper). This corresponds to a period of extensive dissolution (Gvirtzman et al., 2017) coupled with marine regression and subareal exposure along the basin margin (Bertoni & Cartwright, 2007), with wave action (Bache et al., 2012) which all contributed to the shape of the BNM—Base of Nahar Menashe Unit and equivalent to the Intra-Messinian Unconformity Surface. This is also equivalent to the Messinian Unconformity in Sicily (Butler et al., 1995) or the Top Evaporite Unconformity recognized by Bertoni and Cartwright (2007). The previously deposited marginal gypsum and platform carbonates were subaerially exposed and karstified.

Based on our observations combined with previous work, we propose a simple sequence to explain how the Messinian salinity crisis ended in the north-east Levant Basin, offshore Lebanon.

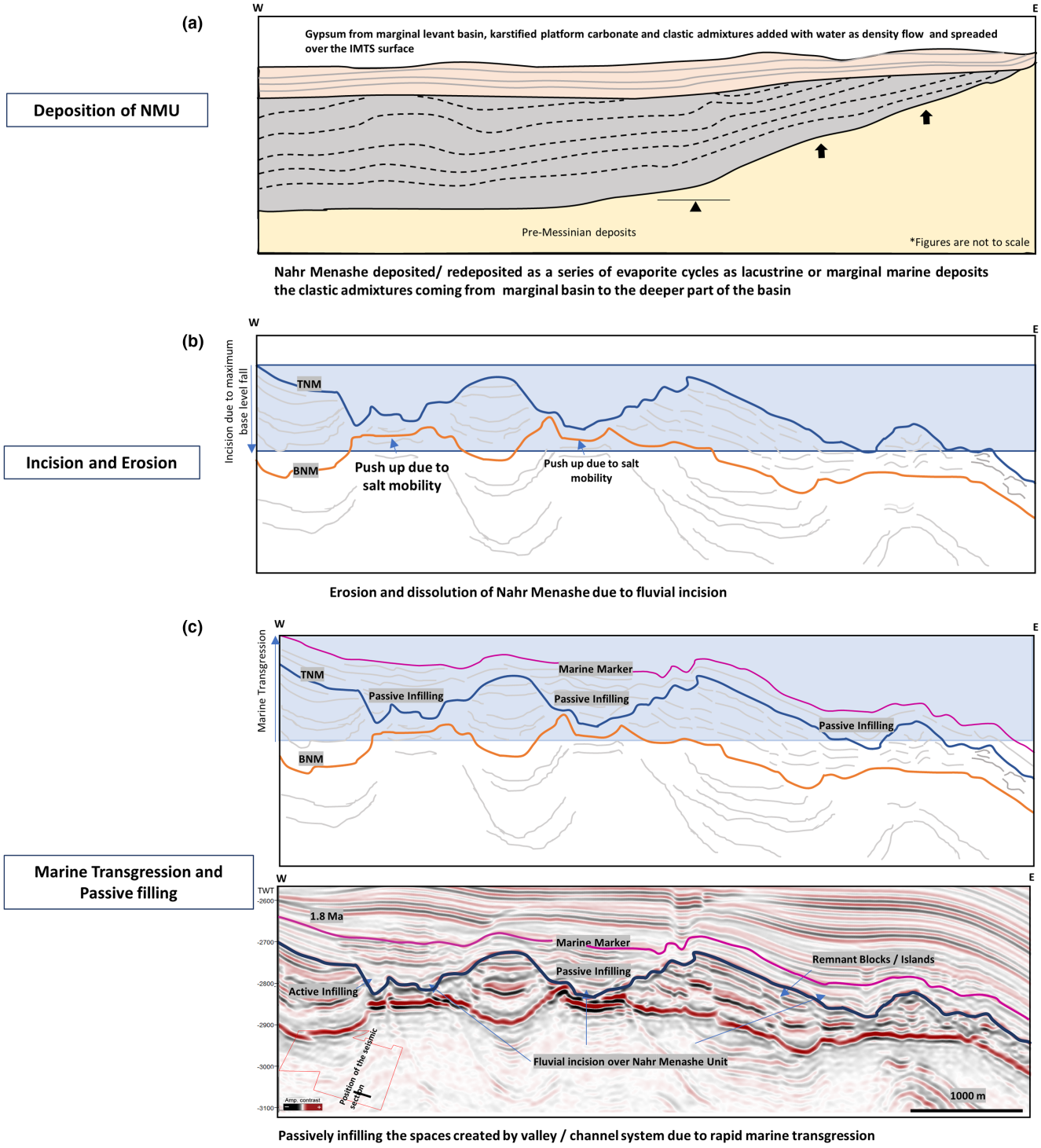

FIGURE 18 MSC termination steps in the north-eastern Levant Basin (a) deposition and/or redeposition of NMU in a lacustrine or marginal marine condition as a series of evaporite cycle, (b) base level dropped down to maximum level and initiation of drainage systems those invaded through the NMU, modified this unit by erosion and dissolution, (c) marine transgression with filling up the erosional spaces.

6.6.1 | Deposition of NMU

After the formation of the dissolution surface recorded by the BNM, the NMU was deposited in a marginal marine or lacustrine setting (or redeposited) as a mixed package of evaporites, carbonates and clastics. Coherent (2–3 cycles) and parallel seismic reflection pattern in the well preserved and undeformed NMU sections clearly indicates the continuation of the evaporite depositional history. The close resemblance of the seismic signatures of the NMU with the lower units of the Messinian evaporites along with the intense dissolution indicators within the

top part of the NMU indicate that the unit consists of several redeposited packages probably characterized by basin centre evaporites, basin marginal gypsum and platform carbonates with clastics derived from both the Lebanon Highlands and the Latakia Ridge all of which were deposited before incision associated with widespread drainage system development (Figure 18a). This is possibly equivalent to the upper MSC stage 3.1 (Meilijson et al., 2019). In this period, the tectonic uplift registered in the slope may have triggered the initial salt flowing mechanism producing the first intra-salt deformation and redeposit of the NMU along the margin slope.

6.6.2 | Incision and erosion

Deposition of the NMU was terminated due to the final and maximum lowering of water level in the reduced and marginally dried up the eastern Mediterranean. In response to this base-level fall, an extensive southerly directed drainage network was established across the entire study area which was continuously affected by mostly subaerial dissolution processes (karst) and erosion. Incision occurred in the NMU leaving relict topographic highs with the dissolution of NM deposits in other areas. This probably represents the final phase of the MSC (3.2) in the north-east Mediterranean. (Figure 18b). This event dramatically reshaped the NMU, contributing to its laterally variable thickness and facies distribution.

6.6.3 | Marine transgression and passive filling

A rapid marine transgression reflooded the basin as the reconnection between the Atlantic and the Mediterranean (Haq et al., 2020) became established and produced parallel and horizontal (vertical stacking) to sub-horizontal (lateral stacking) seismic reflections within the valley and channel system. These units are here interpreted as the first expression of the Zanclean marine reflooding (Andreetto et al., 2021). Seismic reflections appear to onlap or drape against the eroded edges of the remnant blocks of Nahr Menashe stratigraphy or cover the interfluve areas. The geometry and reflection characteristics indicate that the topography was passively infilled (Figure 18c) probably due to rapid flooding and/or marine transgression. The rapid flooding combined with the post-mid-Messinian tectonic compression and gradual uplift caused salt-detached gravity gliding which triggered further salt flowage (Gvirtzman et al., 2013; Oppo et al., 2020). Salt flowage contributed to creating kinematically linked domains parallel to the basin margin, from the slope towards the basin centre: (a) extensional, characterized by margin parallel growth faults which affected the NMU and the post-NMU deposits (this is where we observe Facies 1); (b) translational, with little or null deformation of the overburden (which is where the NMU is better expressed by facies 3–5); (c) contractional, with widespread folding of both the salt and the overburden which affect the NMU and develop facies 6. The pink reflection (considered the first widespread continuous reflection after marine transgression, marine marker) also forms an erosional surface (onlap or truncation of the lower reflections, Figures 11 and 17) following the initial transgression. The age of this event is relatively constrained by its older stratigraphic relationship to the 1.8 Ma event horizon mapped by Kirkham et al. (2020) and interpolated through our seismic dataset.

7 | CONCLUSION

By interpreting high-resolution 3D seismic data and producing detailed mapping across the NMU, we can unravel some depositional aspects which relate to the final stages of the MSC across the Lebanese region of the Levant Basin. The following results were obtained:

- Six seismic facies characterizing the NMU are documented which indicate that it represents a laterally complex redeposited and multilayer brittle–ductile unit.
- The internal architecture of some of the internal NMU reflections represents deposited or redeposited layered mixed clastics and carbonates derived from both the Lebanon Highlands and the Latakia Ridge, in a context of lacustrine or very shallow marine depositional system. The internal reflectivity indicates that it represents a multilayered evaporitic sequence characterized by alternating halite, basin marginal gypsum and clastics derived from platform carbonate subunits.
- All the internal reflectors of the NMU are clearly affected by the widespread presence of linear, semicircular dissolution features and residual mound structures. Their geometry and dimensions suggest that they could represent karsts and dissolution breccias associated with meteoric waters produced during the major regressive event The lack of core or well log data prevents further testing of this hypothesis.
- After NMU deposition a complex, north-to south-trending drainage system was incised into the top of the NMU. The Plio-Quaternary units above the TNM show a seismic facies expression of finely layered units onlapping or infilling the erosive features. These deposits are interpreted to be primarily marine in origin, related to a rapid marine transgression which passively infilled the channel and the valley systems cut into the TNM. These

units are interpreted as the first expression of Zanclean marine reflooding (Andreetto et al., 2021).

- Our analysis suggests that the maximum base level during Messinian times did not drop below the level of the BNM. The drainage network was initiated after deposition and/or redeposition of the NMU, recording erosional rather than deposition and was passively infilled by later marine transgression.
- Our seismic mapping adds further details to the current understanding of the significance of the NMU. The NMU represents a longer and stratigraphically more complex event as indicated by the laterally heterogeneous seismic facies which point to a shallow (periodically evaporative), water environment that developed during the lowstand event and affected the entire Levantine basins prior to subsequent drainage network development. This was followed by a rapid transgressive event that infilled the erosive network and then flooded the entire Lebanon offshore basin.

ACKNOWLEDGEMENTS

We gratefully acknowledge Ramadan Ghalayini, Wissam Chbat and the Lebanese Petroleum Administration (LPA) for the provision of data without which this project would not have been possible. Schlumberger for granting Petrel© academic licences. SM Kabir is expressing his sincere thanks to the Bangabandhu Fellowship Trust, Bangladesh for sponsoring his PhD grant. We thank C. Gorini for the fruitful discussion during wring of this paper. We also thank the editor of the journal and reviewers Madof, Camerlenghi, Patruno and Amadori, who have spent their valuable time enhancing and improving the scientific content of this paper.

PEER REVIEW

The peer review history for this article is available at https://publons.com/publon/10.1111/bre.12697.

DATA AVAILABILITY STATEMENT

The data that support the findings of this study are available from the corresponding author upon reasonable request.

ORCID

David Iacopini https://orcid.org/0000-0003-4925-9665
Adrian Hartley https://orcid.org/0000-0002-5799-4734
Vittorio Maselli https://orcid.org/0000-0001-7301-0769
Davide Oppo https://orcid.org/0000-0002-2866-1498

REFERENCES

Amadori, C., Garcia-Castellanos, D., Toscani, G., Sternai, P., Fantoni, R., Ghielmi, M., & Di Giulio, A. (2018). Restored topography of the Po Plain-Northern Adriatic region during the Messinian base-level drop—Implications for the physiography and compartmentalization of the palaeo-Mediterranean basin. *Basin Research*, *30*(6), 1247–1263.

Andreetto, F., Aloisi, G., Raad, F., Heida, H., Flecker, R., Agiadi, K., Lofi, J., Blondel, S., Bulian, F., Camerlenghi, A., Caruso, A., Ebner, R., Garcia-Cstellanos, D., Gullier, V., Guibourdenche, L., Gvirtzman, Z., Houyle, T. T., Meijer, P. T., Moneron, J., … Krijgsman, W. (2021). Freshening of the Meditteranean salt giant: Controversies and certainties around the terminal (Upper Gypsum and Lago Mare) phases of the Messinian salinity crisis. *Earth Science Review*, *216*, 103577.

Bache, F., Popescu, S. M., Rabineau, M., Gorini, C., Suc, J. P., Clauzon, G., Olivet, J. L., Rubino, J. L., Melinte-Dobrinescu, M. C., Estrada, F., Londeix, L., Armijo, R., Meyer, B., Jolivet, L., Jouannic, G., Leroux, E., Aslanian, D., dos Reis, A. T., Mocochain, L., … Çakir, Z. (2012). A two-step process for the reflooding of the Mediterranean after the Messinian salinity crisis. *Basin Research*, *24*(2), 125–153. https://doi.org/10.1111/j.1365-2117.2011.00521.x

Barnes, A. E., editor. (2016). *Handbook of poststack seismic attributes*. Society of Exploration Geophysicists.

Ben Moshe, L., Ben-Avraham, Z., Enzel, Y., & Schattner, U. (2020). Estimating drawdown magnitudes of the Mediterranean Sea in the Levant basin during the Lago Mare stage of the Messinian salinity crisis. *Marine Geology*, *427*, 106215. https://doi.org/10.1016/j.margeo.2020.106215

Bertoni, C., & Cartwright, J. A. (2007). Major erosion at the end of the Messinian salinity crisis: Evidence from the Levant Basin, Eastern Mediterranean. *Basin Research*, *19*(1), 1–18. https://doi.org/10.1111/j.1365-2117.2006.00309.x

Bertoni, C., & Cartwright, J. (2015). Messinian evaporites and fluid flow. *Marine and Petroleum Geology*, *66*, 165–176.

Beydoun, Z. R. (1999). Evolution and development of the Levant (dead sea rift) transform system: A historical-chronological review of a structural controversy. http://sp.lyellcollection.org

Bowman, S. A. (2011). Regional seismic interpretation of the hydrocarbon prospectivity of offshore Syria. *GeoArabia*, *16*(3), 95–124.

Brown, A. R. (2004). *Interpretation of three-dimensional seismic data*. American Association of Petroleum Geologists and the Society of Exploration Geophysicists.

Burberry, C. M., Jackson, C. A. L., & Chandler, S. R. (2016). Seismic reflection imaging of karst in the Persian Gulf: Implications for the characterization of carbonate reservoirs. *AAPG Bulletin*, *100*(10), 1561–1584. https://doi.org/10.1306/04151615115

Butler, R. W. H., Lickorish, W. H., Grasso, M., Pedley, H. M., & Ramberti, L. (1995). Tectonics and sequence stratigraphy in Messinian basins, Sicily: Constraints on the initiation and termination of the Mediterranean salinity crisis. *GSA Bulletin*, *107*(4), 425–439.

Camerlenghi, A., del Ben, A., Hübscher, C., Forlin, E., Geletti, R., Brancatelli, G., Micallef, A., Saule, M., & Facchin, L. (2019). Seismic markers of the Messinian salinity crisis in the deep Ionian Basin. *Basin Research*, *32*(4), 716–738. https://doi.org/10.1111/bre.12392

Cartwright, J. A., & Jackson, M. P. A. (2008). Initiation of gravitational collapse of an evaporite basin margin: The Messinian saline giant, Levant Basin, eastern Mediterranean. *Bulletin of the Geological Society of America*, *120*(3–4), 399–413. https://doi.org/10.1130/B26081X.1

Cartwright, J., Jackson, M., Dooley, T., & Higgins, S. (2012). Strain partitioning in gravity-driven shortening of a thick, multilayered evaporite sequence. *Geological Society Special Publication*, *363*(1), 449–470. https://doi.org/10.1144/SP363.21

Cartwright, J., Stewart, S., & Clark, J. (2001). *Salt dissolution and salt-related deformation of the Forth Approaches Basin, UK North Sea*. www.elsevier.com/locate/marpetgeo

Chiesi, M., de Waele, J., & Forti, P. (2010). Origin and evolution of a salty gypsum/anhydrite karst spring: The case of Poiano (Northern Apennines, Italy). *Hydrogeology Journal*, *18*(5), 1111–1124. https://doi.org/10.1007/s10040-010-0576-2

Chopra, S., & Marfurt, K. S. (2007). *Seismic attributes for prospect identification and reservoir characterization*. Society of Exploration Geophysicists and European Association of Geoscientists and Engineers.

Druckman, Y., Buchbinder, B., Martinotti, G. M., Siman Tov, R., & Aharon, B. P. (1995). The buried Afiq Canyon (eastern Mediterranean, Israel): A case study of a Tertiary submarine canyon exposed in Late Messinian times. *Marine Geology*, *123*, 167–185.

Evans, S., & Jackson, C. A. (2019). Intrasalt structure and strain partitioning in layered evaporites: Insights from the Messinian salt in the eastern Mediterranean. 81st EAGE Conference and Exhibition 2019. https://doi.org/10.3997/2214-4609.201900911

Feng, Y. E., Yankelzon, A., Steinberg, J., & Reshef, M. (2016). Lithology and characteristics of the Messinian evaporite sequence of the deep Levant Basin, Eastern Mediterranean. *Marine Geology*, *376*, 118–131. https://doi.org/10.1016/j.margeo.2016.04.004

Frey-Martínez, J., Cartwright, J., & James, D. (2006). Frontally confined versus frontally emergent submarine landslides: A 3D seismic characterisation. *Marine and Petroleum Geology*, *23*(5), 585–604.

Gardosh, M. A., & Druckman, Y. (2005). *Seismic stratigraphy, structure and tectonic evolution of the Levantine Basin, offshore Israel*. http://sp.lyellcollection.org/

Gardosh, M., Druckman, Y., Buchbinder, B., & Rybakov, M. (2008). *The Levant Basin offshore Israel: Stratigraphy, structure, tectonic evolution and implications for structure, tectonic evolution and implications for hydrocarbon exploration*. Israel Geological Survey Report.

Gardosh, M. A., Garfunkel, Z., Druckman, Y., & Buchbinder, B. (2010). Tethyan rifting in the Levant region and its role in early Mesozoic crustal evolution. *Geological Society Special Publication*, *341*, 9–36. https://doi.org/10.1144/SP341.2

Gardosh, M. A., & Tannenbaum, E. (2014). The petroleum systems of Israel. In L. Marlow, C. Kendall, & L. Yose (Eds.), *Petroleum systems of the Tethyanregion: AAPG Memoir* (Vol. *106*, pp. 179–216). AAPG Special.

Garfunkel, Z. (1998). Constrains on the origin and history of the Eastern Mediterranean basin. *Tectonophysics*, *298*, 5–35.

Ghalayini, R., Daniel, J. M., Homberg, C., Nader, F. H., & Comstock, J. E. (2014). Impact of Cenozoic strike-slip tectonics on the evolution of the northern Levant Basin (offshore Lebanon). *Tectonics*, *33*(11), 2121–2142. https://doi.org/10.1002/2014TC0035742014

Ghalayini, R., Nader, F. H., Bou Daher, S., Hawie, N., & Chbat, W. E. (2018). Petroleum systems of Lebanon: An update and review. *Journal of Petroleum Geology*, *41*(2), 189–214. https://doi.org/10.1111/jpg.12700

Gradmann, S., Hübscher, C., Ben-Avraham, Z., Gajewski, D., & Netzeband, G. (2005). Salt tectonics off northern Israel. *Marine and Petroleum Geology*, *22*(5), 597–611. https://doi.org/10.1016/j.marpetgeo.2005.02.001

Güneş, P., Aksu, A. E., & Hall, J. (2018). Tectonic and sedimentary conditions necessary for the deposition of the Messinian evaporite successions in the eastern Mediterranean: A simple 2D model. *Marine and Petroleum Geology*, *96*, 51–70. https://doi.org/10.1016/j.marpetgeo.2018.05.022

Gutiérrez, F., & Lizaga, I. (2016). Sinkholes, collapse structures and large landslides in an active salt dome submerged by a reservoir: The unique case of the Ambal ridge in the Karun River, Zagros Mountains, Iran. *Geomorphology*, *254*, 88–103.

Gvirtzman, Z., Manzi, V., Calvo, R., Gavrieli, I., Gennari, R., Lugli, S., Reghizzi, M., & Roveri, M. (2017). Intra-Messinian truncation surface in the Levant Basin explained by subaqueous dissolution. *Geology*, *45*(10), 915–918. https://doi.org/10.1130/G39113.1

Gvirtzman, Z., Reshef, M., Buch-Leviatan, O., & Ben-Avraham, Z. (2013). Intense salt deformation in the Levant Basin in the middle of the Messinian salinity crisis. *Earth and Planetary Science Letters*, *379*, 108–119. https://doi.org/10.1016/j.epsl.2013.07.018

Gvirtzman, Z., Reshef, M., Buch-Leviatan, O., Groves-Gidney, G., Karcz, Z., Makovsky, Y., & Ben-Avraham, Z. (2015). Bathymetry of the Levant basin: Interaction of salt-tectonics and surficial mass movements. *Marine Geology*, *360*, 25–39. https://doi.org/10.1016/j.margeo.2014.12.001

Hall, J., Calon, T. J., Aksu, A. E., & Meade, S. R. (2005). Structural evolution of the Latakia Ridge and Cyprus Basin at the front of the Cyprus Arc, Eastern Mediterranean Sea. *Marine Geology*, *221*(1–4), 261–297. https://doi.org/10.1016/j.margeo.2005.03.007

Haq, B., Gorini, C., Baur, J., Moneron, J., & Rubino, J. L. (2020). Deep Mediterranean's Messinian evaporite giant: How much salt? *Global and Planetary Change*, *184*, 103052. https://doi.org/10.1016/j.gloplacha.2019.103052

Hardage, B. A., Carr, D. L., Lancaster, D. E., Simmons, J. L., Elphick, R. Y., Pendleton, V. M., & Johns, R. A. (1996). 3-D seismic evidence of the effects of carbonate karst collapse on overlying clastic stratigraphy and reservoir compartmentalization. *Geophysics*, *61*(5), 1336–1350. https://doi.org/10.1190/1.1444057

Hardy, C., Homberg, C., Eyal, Y., Barrier, É., & Müller, C. (2010). Tectonic evolution of the southern Levant margin since Mesozoic. *Tectonophysics*, *494*(3–4), 211–225. https://doi.org/10.1016/j.tecto.2010.09.007

Hawie, N., Gorini, C., Deschamps, R., Nader, F. H., Montadert, L., Granjeon, D., & Baudin, F. (2013). Tectono-stratigraphic evolution of the northern Levant Basin (offshore Lebanon). *Marine and Petroleum Geology*, *48*, 392–410. https://doi.org/10.1016/j.marpetgeo.2013.08.004

Henderson, J., Purves, S. J., Fisher, G., & Leppard, C. (2008). Delineation of geological elements from RGB color blending of seismic attribute volumes. *The Leading Edge*, *27*(3), 342–350.

Hilton, V. C. (2001). *BG International offshore Israel, Med Yavne license: Or-1 & Or South-1, structural and sedimentological interpretation of STAR data, core sedimentology and petrography of core samples*. Baker Atlas GEOScience *Final Report ZSL-00-075*.

Hsü, K. J., Ryan, W. B. F., & Cita, M. B. (1973). Late miocene desiccation of the Mediterranean. *Nature*, *242*(5395), 240–244. https://doi.org/10.1038/242240a0

Jackson, M. P. A., Vendeville, B. C., & Schultz-Ela, D. D. (1994). *Structural dynamics of salt systems*. www.annualreviews.org

Jackson, M. P., & Hudec, M. R. (2017). *Salt tectonics: Principles and practice*. Cambridge University Press.

Jaworska, J., & Nowak, M. (2013). Anhydrites from gypsum cap-rock of Zechstein salt diapirs. *Geology, Geophysics & Environment*, *39*(3), 233. https://doi.org/10.7494/geol.2013.39.3.233

Jilinski, P., & Wooltorton, T. (2016). Comparison of spectral enhancement techniques and application to improved well-to-seismic ties. *GeoConvention*, *2016*, 1–4.

Kartveit, K. H., Omosanya, K. O., Johansen, S. E., Eruteya, O. E., Reshef, M., & Waldmann, N. D. (2018). Multiphase structural evolution and geodynamic implications of Messinian salt-related structures, Levant Basin, offshore Israel. *Tectonics*, *37*(5), 1210–1230. https://doi.org/10.1029/2017TC004794

Kartveit, K. H., Ulsund, H. B., & Johansen, S. E. (2019). Evidence of sea level drawdown at the end of the Messinian salinity crisis and seismic investigation of the Nahr Menashe unit in the northern Levant Basin, offshore Lebanon. *Basin Research*, *31*(5), 827–840. https://doi.org/10.1111/bre.12347

Kirkham, C., Bertoni, C., Cartwright, J., Lensky, N. G., Sirota, I., Rodriguez, K., & Hodgson, N. (2020). The demise of a 'salt giant' driven by uplift and thermal dissolution. *Earth and Planetary Science Letters*, *531*, 115933. https://doi.org/10.1016/j.epsl.2019.115933

Kirkham, C., Cartwright, J., Hermanrud, C., & Jebsen, C. (2017). The spatial, temporal and volumetric analysis of a large mud volcano province within the Eastern Mediterranean. *Marine and Petroleum Geology*, *81*, 1–16. https://doi.org/10.1016/j.marpetgeo.2016.12.026

Kyle, J. R., & Posey, H. H. (1991). *Halokinesis, cap rock development, and salt dome mineral resources*. Elsevier.

Lazar, M., Lang, G., & Schattner, U. (2016). Coincidence or not? Interconnected gas/fluid migration and ocean–atmosphere oscillations in the Levant Basin. *Geo-Marine Letters*, *36*(4), 293–306. https://doi.org/10.1007/s00367-016-0447-5

Lebedeva-Ivanova, N., Polteau, S., Bellwald, B., Planke, S., Berndt, C., & Stokke, H. H. (2018). Toward one-meter resolution in 3D seismic. *The Leading Edge*, *37*(11), 818–828.

Lofi, J., Sage, F., Déverchère, J., Loncke, L., Maillard, A., Gaullier, V., Thinon, I., Gillet, H., Guennoc, P., & Gorini, C. (2011). Refining our knowledge of the Messinian salinity crisis records in the offshore domain through multi-site seismic analysis. *Bulletin de la Société géologique de France*, *182*(2), 163–180.

Madof, A. S., Bertoni, C., & Lofi, J. (2019). Discovery of vast fluvial deposits provides evidence for drawdown during the late Miocene Messinian salinity crisis. *Geology*, *47*(2), 171–174. https://doi.org/10.1130/G45873.1

Maillard, A., Hübscher, C., Benkhelil, J., & Tahchi, E. (2011). Deformed Messinian markers in the Cyprus Arc: Tectonic and/or Messinian salinity crisis indicators? *Basin Research*, *23*(2), 146–170. https://doi.org/10.1111/j.1365-2117.2010.00464.x

Manzi, V., Gennari, R., Hilgen, F., Krijgsman, W., Lugli, S., Roveri, M., & Sierro, F. J. (2013). Age refinement of the Messinian salinity crisis onset in the Mediterranean. *Terra Nova*, *25*(4), 315–322.

Matmon, A., Enzel, Y., Zilberman, E., & Heimann, A. (1999). Late Pliocene and Pleistocene reversal of drainage systems in northern Israel: Tectonic implications. *Geomorphology*, *28*, 43–59.

Meilijson, A., Hilgen, F., Sepúlveda, J., Steinberg, J., Fairbank, V., Flecker, R., Waldmann, N. D., Spaulding, S. A., Bialik, O. M., Boudinot, F. G., Illner, P., & Makovsky, Y. (2019). Chronology with a pinch of salt: Integrated stratigraphy of Messinian evaporites in the deep Eastern Mediterranean reveals long-lasting halite deposition during Atlantic connectivity. *Earth-Science Reviews*, *194*, 374–398. https://doi.org/10.1016/j.earscirev.2019.05.011

Micallef, A., Camerlenghi, A., Georgiopoulou, A., Garcia-Castellanos, D., Gutscher, M. A., Lo Iacono, C., Huvenne, V. A. I., Mountjoy, J. J., Paull, C. K., le Bas, T., Spatola, D., Facchin, L., & Accettella, D. (2019). Geomorphic evolution of the Malta Escarpment and implications for the Messinian evaporative drawdown in the eastern Mediterranean Sea. *Geomorphology*, *327*, 264–283. https://doi.org/10.1016/j.geomorph.2018.11.012

Nader, F. H. (2011). The petroleum prospectivity of Lebanon: An overview. *Journal of Petroleum Geology*, *34*(2), 135–156. https://doi.org/10.1111/j.1747-5457.2011.00498.x

Netzeband, G. L., Hübscher, C. P., & Gajewski, D. (2006). The structural evolution of the Messinian evaporites in the Levantine Basin. *Marine Geology*, *230*(3–4), 249–273. https://doi.org/10.1016/j.margeo.2006.05.004

Niyazi, Y., Eruteya, O. E., Omosanya, K. O., Harishidayat, D., Johansen, S. E., & Waldmann, N. (2018). Seismic geomorphology of submarine channel-belt complexes in the Pliocene of the Levant Basin, offshore central Israel. *Marine Geology*, *403*, 123–138. https://doi.org/10.1016/j.margeo.2018.05.007

Oppo, D., Evans, S., Iacopini, D., Mainul Kabir, S. M., Maselli, V., & Jackson, C. A.-L. (2021). Leaky salt: Pipe trails record the history of cross-evaporite fluid escape in the northern Levant Basin, Eastern Mediterranean. *Basin Research*, *33*(3), 1798–1819.

Petrolink, G., Brew, G., Barazangi, M., Al-Maleh, A. K., & Sawaf, T. (2001). Tectonic and geologic evolution of Syria. *GeoArabia*, *6*(4), 573–616. http://pubs.geoscienceworld.org/geoarabia/article-pdf/6/4/573/4560629/brew.pdf

Popescu, S. M., Cavazza, W., Suc, J. P., Melinte-Dobrinescu, M. C., Barhoun, N., & Gorini, C. (2021). Pre-Zanclean end of the Messinian salinity crisis: New evidence from central Mediterranean reference sections. *Journal of the Geological Society*, *178*(3), jgs2183.

Robertson, A. H. (1998). Mesozoic-tertiary tectonic evolution of the easternmost Mediterranean area: Integration of marine and land evidence. Proceedings of the Ocean drilling program, Scientific Results (Vol. *160*). Chapter 54.

Robertson, A. H. F., Parlak, O., & Ustaömer, T. (2012). overview of the Palaeozoic—Neogene evolution of neotethys in the Eastern Mediterranean region (southern Turkey, Cyprus, Syria). *Petroleum Geoscience*, *18*(2004), 381–404. https://doi.org/10.1144/petgeo2011-091.1354-0793/12/

Rodriguez, C. R., Jackson, C. A.-L., Bell, R. E., Rotevatn, A., & Francis, M. (2018). *Submarine salt dissolution in the Santos Basin, offshore*. EarthArXiv. https://doi.org/10.31223/osf.io/en4x7

Roveri, M., Gennari, R., Lugli, S., Manzi, V., Minelli, N., Reghizzi, M., Riva, A., Rossi, M. E., & Schreiber, B. C. (2016). The Messinian salinity crisis: Open problems and possible implications for Mediterranean petroleum systems. *Petroleum Geoscience*, *22*(4), 283–290. https://doi.org/10.1144/petgeo2015-089

Roveri, M., Lugli, S., Manzi, V., Gennari, R., & Schreiber, B. C. (2014). High-resolution strontium isotope stratigraphy of the Messinian deep Mediterranean basins: Implications for marginal to central basins correlation. *Marine Geology*, *349*, 113–125.

Ryan, W. B. (2011). Geodynamic responses to a two-step model of the Messinian salinity crisis. *Bulletin de la Société Géologique de France*, *182*(2), 73–78.

Ryan, W. B. F. (1978). Messinian badlands on the southeastern margin of the Mediterranean sea. *Marine Geology*, *27*, 349–363.

Ryan, W. B. F., & Cita, M. B. (1978). The nature and distribution of Messinian erosional surfaces—Indicators of a several-kilometer-deep Mediterranean in the miocene. *Marine Geology*, *27*, 193–230.

Ryan, W. B. F., Hsu, K. J., Cita, M. B., Dumitrica, P., Lort, J., Maync, W., Nesterhoff, W. D., Pautot, G., Stradner, H., & Wezel, L. F. C. (1973). Western Alboran basin-site 121. *Initial Reports of the Deep Sea Drilling Project*, *13*, 43–49.

Stafford, K. W., Nance, R., Rosales-Lagarde, L., Boston, P. J., Stafford, K. W., Nance, R., Rosales-Lagarde, L., & Epigene and Hypogene Gypsum Karst. (2008). *Repository citation repository citation epigene and hypogene gypsum karst manifestations of the castile formation: Eddy county, New Mexico and Culberson County, Texas, USA*. https://scholarworks.sfasu.edu/geology/12

Vidal, N., Alvarez-Marrö N Ay, J., & Klaeschen, D. (2000). *Internal configuration of the Levantine Basin from seismic reflection data (eastern Mediterranean)*. www.elsevier.com/locate/epsl

Walley, C. D. (1997). The lithostratigraphy of Lebanoni a reriew. *Lebonese Science Bulletin*, *10*, 81–108.

Zeng, H., Wang, G., Janson, X., Loucks, R., Xia, Y., Xu, L., & Yuan, B. (2011). Characterizing seismic bright spots in deeply buried, Ordovician Paleokarst strata, Central Tabei uplift, Tarim Basin, Western China. *Geophysics*, *76*(4), B127–B137. https://doi.org/10.1190/1.3581199

Zucker, E., Gvirtzman, Z., Granjeon, D., Garcia-Castellanos, D., & Enzel, Y. (2021). The accretion of the Levant continental shelf alongside the Nile Delta by immense margin -parallel sediment transport. *Marine and Petroleum Geology*, *126*, 2021.

How to cite this article: Kabir, S. M. M., Iacopini, D., Hartley, A., Maselli, V., & Oppo, D. (2022). Seismic characterization and depositional significance of the Nahr Menashe deposits: Implications for the terminal phases of the Messinian salinity crisis in the north-east Levant Basin, offshore Lebanon. *Basin Research*, *00*, 1–26. https://doi.org/10.1111/bre.12697